1-1-2018

Generalized DOA and Source Number Estimation Techniques for Acoustics and Radar

Emily Erin Gorman

Generalized DOA and source number estimation techniques for acoustics and radar

By

Emily Erin Gorman

A Thesis
Submitted to the Faculty of
Mississippi State University
in Partial Fulfillment of the Requirements
for the Degree of Master of Science
in Electrical and Computer Engineering
in the Department of Computer Science and Engineering

Mississippi State, Mississippi

May 2018

Generalized DOA and source number estimation techniques for acoustics and radar

By

Emily Erin Gorman

Approved:

John E. Ball
(Major Professor)

Bo Tang
(Committee Member)

Anton Netchaev
(Committee Member)

James E. Fowler
(Graduate Coordinator)

Jason M. Keith
Dean
Bagley College of Engineering

Name: Emily Erin Gorman

Date of Degree: May 4, 2018

Institution: Mississippi State University

Major Field: Electrical and Computer Engineering

Major Professor: John E. Ball

Title of Study: Generalized DOA and source number estimation techniques for acoustics and radar

Pages of Study: 79

Candidate for Degree of Master of Science

The purpose of this thesis is to emphasize the lacking areas in the field of direction of arrival estimation and to propose building blocks for continued solution development in the area. A review of current methods are discussed and their pitfalls are emphasized. DOA estimators are compared to each other for usage on a conformal microphone array which receives impulsive, wideband signals. Further, many DOA estimators rely on the number of source signals prior to DOA estimation. Though techniques exist to achieve this, they lack robustness to estimate for certain signal types, particularly in the case where multiple radar targets exist in the same range bin. A deep neural network approach is proposed and evaluated for this particular case. The studies detailed in this thesis are specific to acoustic and radar applications for DOA estimation.

DEDICATION

The work in this thesis is dedicated to my fiancé, Paul Leathers, who recognizes my ability to see through the end of everything I start in life, and my parents, Berry and Lisa Gorman, who have always told me I can achieve anything I set my mind to. Their love and support have enabled me to pursue my dreams.

ACKNOWLEDGEMENTS

I thank the United States' Office of Personel Management and the National Science Foundation for funding my continued education through the Cybercorps Scholarship for Service.

I would like to extend special appreciation to the US Army Corps of Engineers Engineering Research and Development Center and my mentor, Dr. Anton Netchaev, for inspiring this research and introducing me to a career in this field of study.

I further would like to thank my classmate, John Rogers for his contributions in this study regarding number of source estimations.

Finally, I thank my committee for their feedback and suggestions on this thesis. I especially thank my major professor, Dr. John E. Ball for overseeing this research, for his continued patience and encouragement, and for his contributions to the proposed deep neural network in this work.

TABLE OF CONTENTS

LIST OF TABLES

LIST OF FIGURES

CHAPTER I

INTRODUCTION

1.1 Motivation

Direction of arrival (DOA) estimation is relevant in acoustics, radar, sonar, and wireless applications and has been widely studied for the past several decades. Being able to approximately localize a source or target contributes to environmental awareness and more detailed scene understanding necessary for modern-world applications which rely heavily on sensor-gathered information. This is particularly useful for autonomous vehicles which rely on being able to fully understand a dynamic environment without reliance on human direction. DOA is also applicable in military applications where it may be advantageous to know where a blast originated from or where a particular target exists, for both offensive and defensive purposes. Determining the DOA from a sensor array is significant in that it can be done in circumstances where a-priori knowledge is unknown and in settings where it is impractical or unsafe for the determination to be made by a person.

From multiple sensor arrays, a source can be confidently localized to a position in space, through triangulation of combined arrays estimates of directionality. Often these multiple sensor arrays are distributed such that significant distance exists between them. As such, the case where a sufficiently-distanced source signal only reaches a singular sensor array presents a challenge in resolving the location of the source. However, for cases

where only a single sensor array can be utilized, it is necessary to still be able to determine the origin of the source and thus alternative approximations must be employed. From a relatively small (small in that the elements are not distributed such that they are representative of several larger distributed arrays), singular array configuration, the ability to localize a source is limited to determining the general directionality of arrival, respective to the sensor array, and is also limited by the number of array elements. Depending on the application, elements of phased arrays are spaced with the wavelength of the signal in mind such that smaller waves such as radio waves require smaller array apertures than those of acoustics.

In the context of this work, the DOA is characterized as the relative angular projection of a given source signal onto an appropriate receiving array. Though both azimuth (θ) and elevation (ϕ) arrival angles can be extracted from source signal information, there is particular interest in being able to know only the general azimuth directionality for localization purposes.

Array configurations significantly affect an estimator's ability to approximate an appropriate angle. Most studied array geometries are uniformly-spaced, despite recent studies which have shown arbitrarily-spaced elements to provide a more robust reception [55]. Furthermore, the inclusion for wideband acoustic signals has not been heavily integrated into the literature. There exist approaches which exploit the separation of a wideband signal into frequency bins such that narrowband methods can be utilized [55]. Even so, many popular estimators rely on prior knowledge of the number of source signals to compute ap-

propriate DOAs. Because this information is difficult to know in a real-world application, additional data analysis techniques are necessary to make this prediction.

Source number estimation techniques which work reasonably well have been implemented and used for varied applications. However, in a particular case of radar application, most of these methods based on signal subspace exploitation are insufficient to properly estimate the number of received signals.

Thus, this thesis was motivated by developing contributing work in the area of direction of arrival estimation for both acoustic and radar applications. The ultimate goal of this thesis was to work towards the development of a solution for robust DOA estimation on an arbitrary sensor array, given a wideband signal.

1.2 Applications

DOA estimation is applicable in several areas of array signal processing to include acoustics, radar, and sonar. These applications vary in their specific details like propagation properties and equipment variances but ultimately can be reduced to the same foundational components. Typical applications for DOA estimation include source localization, target detection, and object tracking.

To appropriately estimate the DOA of a given signal, it is assumed that there exists some sensor array which receives a signal of interest in the presence of noise and a processing algorithm uses such data to estimate the DOA.

In acoustic applications, DOA estimation can be used to determine the source location of a sound. This information is relevant to scene understanding as well as source track-

ing. In radar applications, it is often advantageous to be able to recognize the presence or absence of a specified target in the surrounding environment.

Current studies in the area focus on determining the DOA of moving sources, moving receiver arrays, or a combination of both. However, the scope of this research is limited to stationary sources and receiver arrays. Thus, due to added uncertainty and increased complexity of non-stationary signal emmition and reception, the studies herein are not directly applicable to dynamic components.

Though DOA estimation is applicable to both compact and distributed arrays, the experiments done through the course of this work were focused on considerably compact array geometries with a notably small number of sensor elements. Thus, the implications of this study are not necessarily indicative of usage on a sizeable array geometry with higher numbers of receiving sensors.

This work emphasizes the applications of real-world acoustic data and simulated radar data. As such, the application of these methods can be done for both simulated and experimental datasets. It should be noted that real-world data is subject to additional external influence than may be accounted for by simulated signals. Techniques perform optimally in simulations of idealized signals and degrade in their performance for real-world applications where signals are subject to interference.

1.3 Work Overview

The work detailed herein applies to the development of improved and more robust techniques for DOA estimation. These contributions were exploratory discoveries as well as

technique advancements. The scope of this study is not limited to a singular application and is rather a culmination of three individual studies which all contribute to the advancement of DOA estimation techniques.

Throughout the course of this work, it was learned that there are several lacking areas in the field of DOA estimation techniques. Though there exist widely-used techniques throughout the literature, these techniques are limited by their capacity to work with certain signal expectations and array configurations.

For the case where wideband signals arrive to an irregular array geometry, there are few methods designed for that application. Two methods- generalized cross correlation (GCC) and unconstrained least squares (ULS) were compared against one another for efficacy on varied wideband acoustic sources. This study also examines the effects of using sub-arrays of the irregular geometry.

Many other DOA estimators rely upon knowing the number of sources a priori to angle estimation [45, 49]. In trying to improve upon number of source estimation techniques for a radar application where all target signals exist in the same range bin, it was discovered that there lacks an effective method which does not rely on eigenvalue decomposition to estimate the number of sources. This discovery was found during the attempted development of a neural network that exploits the eigenvalues to estimate the number of sources. Given a particular set of radar data, the commonly-used methods were shown ineffective, as was the proposed network. However, given different input data, the methods were sufficiently able to make the determination, thus exposing the problematic case where targets exist in the same range bin.

After evaluating that eigenvalue decomposition is insufficient for number of source estimations, given the specific radar case, a deep neural network (NN) was developed as a solution to this problem. The NN was created such that it relies on both the eigenvalues as well as the covariance matrix to estimate an appropriate number of targets. This novel method was compared against other methods in the literature and found to perform significantly better.

Though a comprehensive and generalized solution is not yet created for a robust DOA estimator, lacking discoveries have been found and milestones achieved to progress development in this area towards a robust and generalized solution.

1.4 Contributions

The contributions in this thesis are relevant to signal processing applications, especially those which are related to array processing and source localization.

The contributions of this thesis are:

1. A study on real-world impulsive acoustic signals for a conformal microphone array geometry.

2. The exposure to a lacking area in number of source detectors for a radar application where signals exist in the same range bin.

3. A proposed neural network that can be used to derive the number of sources detected such that DOA methods which require a robust estimation of this quantity can be utilized.

The study presented in Chapter III has been published as part of the 174th conference of the Acoustical Society of America in the Proceedings of Meetings on Acoustics [20]. The proposed method discussed in Chapter IV has been submitted to IEEE Access and is currently under review for acceptance [21].

1.5 Organization

This thesis is organized in the following manner: Chapter 1 introduces the work of this thesis. Chapter 2 is an extensive literature review that discusses the background relevant to various aspects of DOA estimation. Chapter 3 details the experimentation and findings of statistical DOA estimation techniques for a conformal microphone array on impulsive acoustic sources. Chapter 4 compares the proposition of two neural network approaches to determine the number of targets present in a radar application. Chapter 5 summarizes the contributions of this thesis and lists future work.

CHAPTER II

BACKGROUND

2.1 Beamforming

The areas of most effective reception for a signal are characterized by the beam pattern of a specific array geometry, where the frequency-wavenumber response is computed for all spherical angles about the array [55]. Elements of the array can be adjusted or weighted such that they produce a desired beam pattern through beamforming techniques.

Given a signal received (y) at differing time delays at each element (such that $W(\theta)$ is a weighted vector which is a linear combination of all array elements' signals and H is the Hermitian transpose), with the sensor array geometry known, the beam pattern can be determined when the received signal power (p) of all elements' received signals is strongest at a particular angle, θ

$$p(\theta) = |\mathbf{W}(\theta)^H \mathbf{y}|^2 \tag{2.1}$$

Use of beamforming is important in circumstances where one would like to transmit or receive a signal from a particular direction with the optimal beam pattern. Beamforming is also particularly useful in the case of DOA estimation, since the beam pattern optimally defines the source's DOA, in the absence of noise [55].

2.2 Acoustics

Acoustic signals are those signals which result from the vibration of molecules in a propagation medium, onset initially by the movement of some given source. In most acoustic applications, the sounds of interest are typically that which span a broad spectrum of frequencies, though singular tonal sounds do also exist [55]. These wide bandwidth sounds are characterized by the summation of several singular longitudinal sinusoidal waves over a spread of different amplitudes, phases, and frequencies [34].

Acoustic signals propagate from the initializing source in a cocentric manner, with the sound waves radiating about the source in an outward direction. As the energy travels further from the source of the sound, the waves become progressively less curved. Depending on how close the receptive array is to the source will determine what kind of signal is received.

A signal is said to exist in the near field if the impinging wavefront is characteristic of the circular curve. However, if the receivers are sufficiently separated from the source, the array will see a planar wavefront upon arrival. In the far field, the sound pressure level decreases as a function of the inverse square law [1].

Wideband signals can be complicated further by external influences that act against an idealized signal and propagation model. There are two primary factors which can alter how a signal is received- propagation medium parameters and environmental characteristics.

In the acoustic realm of signal processing, the waves travel at the speed defined by a given propagation medium. For the purposes of this work, air is assumed to be the propagation medium and is subject to variance based on moisture content as well as temperature.

While moisture levels produce a less-pronounced effect on the speed that can be considered negligible for most purposes, the temperature of the medium affects the speed in the following manner: $c = 332 + 0.6T_c$, where c is the propagation speed in meters per second (m/s) and T_c is the temperature in degrees Celsius ($^{\circ}C$). For most standard application, it can be assumed that the propagation speed of a sound through air at $20^{\circ}C$ and 1 atmospheric pressure is $343m/s$ [34].

The signal can be undesirably diminished by the environment in the propagation path surrounding an acoustic event and the reception point. Reverberation and absorption are both unavoidable in any realistic location. As such, the path of the waves are subject to change, causing unwanted delay in a singular event, often so much that an echo may be indistinguishable from a second arrival signal [1]. Obviously, with increased sound sources, this problem becomes progressively more complex.

Moving sources are subject to additional consideration with array processing. With the change in positioning of a sound-generating source, the signal becomes a product of the Doppler affect, which manifests as a frequency change.

2.3 Array Geometries

The most commonly-used array geometries are that of uniformly-distributed nature such as uniform linear arrays and uniform circular arrays, though more complex variations of this uniformity have also been studied (uniform rectangular arrays, uniform planar arrays, uniform spherical arrays, etc.) The least-often used array geometries are those which follow a conformal, or non-uniformly spaced pattern [55, 56, 66, 61].

Array geometries are defined by the placement of the same sensor at various positions in space. They can be 1D, as in the case of linear arrays, 2D as in the case of planar arrays, and 3D as in the case of spherical arrays [56].

The number of sensors plays an important role in the performance of a given geometry. Too few elements does not allow for appropriate resolution, especially in cases where there exist multiple signal sources. Oppositely, too many elements introduce coupling between elements. Ultimately, the design is usually a trade-off between the desired performance, the capacity of the system's computational power, and the cost for such operation [55].

One-dimensional arrays are most often used in array processing and are simply composed of elements in a singular line. Often these arrays are equispaced, where each element is separated by the same distance from each consecutive element though nonuniform spacing has surfaced recently in the literature [29]. Linear arrays are widely known for their simplicity to implement and analyze [56].

Planar, or 2D, arrays are those array geometries which span both the X and Y direction but do not change between the Z direction. Commonly used geometries of this type are uniform circular arrays, uniform rectangular arrays. Circular arrays are desirable in that they can provide uniformity of reception in the beam pattern over a 360 degree field of view [55].

Conformal array geometries are those where elements of the array typically conform to some curved surface and compose a large portion of 3D arrays, where elements are placed in the X,Y, and Z directions, respective to one another [56]. This geometry is not specific to any particular shape or placement and thus can be utilized in cases of randomly placed

elements. Spherical and cylindrical arrays fall into this category. Of the few common conformal arrays, a pyramid/conical shape has shown to perform better than other geometries, specifically in DOA applications [32].

Array geometry design is beyond the scope of this work, though it should be noted how critical the design of the array is for DOA applications, and that each geometry comes with a balance of desirable and undesirable properties.

2.4 DOA Estimation

DOA estimation is determined by how a transmitted signal impinges on a receiving element array. The DOA estimate is characterized by the angular estimate from which the source of the data originated.

As with any array processing, the collected data is subject to outside influences and signal degradation. This propagation is affected by the surrounding environment, propagation medium parameters, and quality of the emitters and receiving elements. Furthermore, signals will always be subject to noise introduced by the environment or the system itself.

Given an array of M elements, the vector of the total received data $x(t)$ can be modeled as

$$x(t) = \begin{bmatrix} s(t-\tau_1)e^{jw_c(t-\tau_1)} \\ s(t-\tau_2)e^{jw_c(t-\tau_2)} \\ \vdots \\ s(t-\tau_M)e^{jw_c(t-\tau_M)} \end{bmatrix} \tag{2.2}$$

where each received signal $s(t - \tau_M)$ at the Mth array element is reflective of the transmitted signal at time τ_M, $e^{jw_c(t-\tau_M)}$ is the phase shift, and $w_c = 2\pi f_c$ such that f_c is the carrier frequency of the signal. The delay of reception for each element is correlated to the angles by which the source initially transmitted the signal [55].

This estimate is typically measured by the azimuth and elevation angles respective to the centroid of the array. The azimuth angle is defined as "the angle in the counter-clockwise direction from the x-axis" and the elevation angle as "the angle computed from the positive z-axis" [55]. This concept is illustrated in Fig. 2.1 and 2.2. Thus, the directionality of a source can be found from any angular combination of the azimuth and elevation or simply from one of these measurements, depending on the resolution necessary. A definitive source localization can be found from the triangulation of several sensor arrays' DOA estimates combined with one another. Otherwise, when a singular sensor array is utilized, DOA estimates are limited to angular estimates and not a particular location defined by distance.

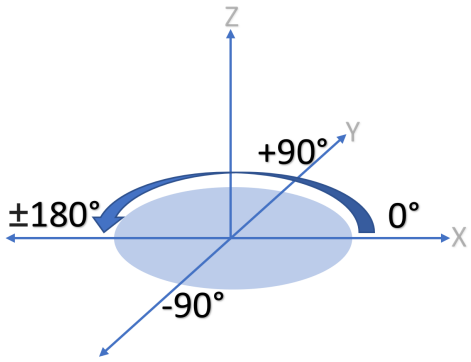

Figure 2.1: Visualization of azimuth angle measurements.

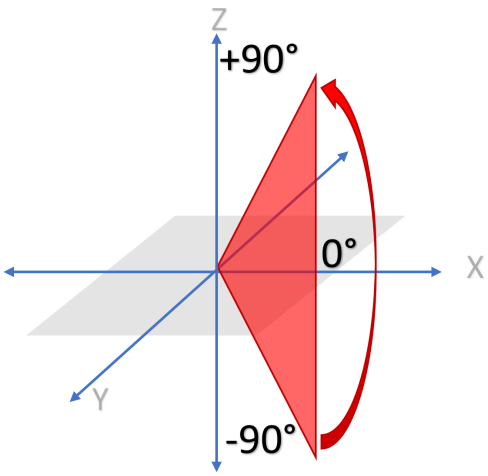

Figure 2.2: Visualization of elevation angle measurements.

The array is characterized by a, the array manifold, which describes the directional properties by which each array element operates and is defined by the azimuth ϕ and zenith θ angles such that

$$a(\phi, \theta) = [a_1(\phi, \theta), \ldots, a_N(\phi, \theta)]^T. \tag{2.3}$$

The Cramer Rao bound defines the limitations of which a DOA estimator can effectively estimate a given source's angular location for K snapshots of a signal for the derivative of the array manifold with respect to θ ($\dot{a}(\theta)$)

$$CRB \approx \frac{1}{2K * SNR * |\dot{a}(\theta)|^2}, \tag{2.4}$$

where SNR is the signal-to-noise ratio received at each array element [55].

The mean square error (MSE) is the standard measure of performance for DOA estimators.

Several methods have been proposed and tested for varied array geometries and signal types. The vast majority of these estimators were designed for usage on narrowband signals which impinge a uniformly-spaced arrays.

2.5 Techniques

The most basic means to estimate the DOA of an acoustic signal is by maximum likelihood methods which exploit the time difference of arrivals (TDOA) for a given signal upon each array element. This estimate is often made by determining the maximum correlation of each pair of sensors' received signals to one another and making an angular estimate via a least squares solution. Such approaches exhibited in the generalized cross correlation (GCC) [35] method as well as the unconstrained least squares method (ULS) [6]. Both methods are appropriate for usage on wideband signals as well as irregularly shaped array geometries [55].

The formulation for the GCC $\hat{R}^{(g)}_{y1y2}$ was defined by Knapp and Carter in [35] for signals x_1 and x_2 to be:

$$\hat{R}^{(g)}_{y1y2}(\tau) = \int_{-\infty}^{\infty} \psi_g(f)\hat{G}_{x1x2}(f)e^{j2\pi f\tau}df \tag{2.5}$$

such that $\hat{G}_{x1x2}(f)e^{j2\pi f\tau}$ is the power spectral density function and ψ is defined by

$$\psi_g(f) = H_1(f)H_2^*(f). \tag{2.6}$$

The filters H_1 and H_2 are non-specific to this generalized formulation. For the particular formulation discussed in this thesis, the GCC with Phase Transform (GCC-PHAT) was utilized, where ψ is defined by inverse of the absolute value of the transpose of $G_{x1x2}(f)$ such that

$$\psi_p(f) = \frac{1}{|G_{x1x2}(f)|'}. \tag{2.7}$$

The ULS method is defined as the solution to the linear system of equations in the matrix form Matrix form

$$\phi y = b \tag{2.8}$$

where

$$\phi = \begin{bmatrix} a_1^T & v_1 \\ \vdots & \vdots \\ a_M^T & v_M \end{bmatrix} \quad y = \begin{bmatrix} x \\ r \end{bmatrix} and \quad b = \frac{1}{2} \begin{bmatrix} ||a_1||^2 - c^2\tau_{1,0}^2 \\ \vdots \\ ||a_M||^2 - c^2\tau_{M,0}^2 \end{bmatrix} \tag{2.9}$$

where a_i is the array element positioning for M elements, v is $c\tau_{i,0}$ (propagation speed * TDOA), x is the source location, and r is the source range from the array. The solution for the unknown vector $\hat{y}$ is $\hat{y} = \phi^{\ddagger} b$, where $\phi^{\ddagger}$ is is the pseudo inverse of ϕ

$$\hat{y} = \begin{bmatrix} \hat{x} \\ \hat{r} \end{bmatrix} = (\phi^T \phi)^{-1} \phi^T. \tag{2.10}$$

By defining that the range $\hat{r}$ and positioning $\hat{x}$ of the source location are independent one another, the range byproduct $\hat{r}$ of the linear system of equations can be discarded, thus defining the least squares estimate to be unconstrained by that parameter [27, 6].

Like GCC, the ULS estimate utilizes a linear least squares estimate. The difference in this approach from GCC is that the propagation speed is assumed to be unknown and estimated simultaneously to a definitive source location. Further, it is assumed that the arrays experience the curvature of the acoustic signal against the array elements, as the method is intended for signals occurring in the near field.

Other methods exist which are based on the separation of signal and noise subspaces and subsequently known as subspace methods. Given a received signal, a subspace can be estimated such that the signal subspace is composed of D components, where D is indicative of the number of sources [56]. Because it is impractical for D to be known a priori, this parameter must be estimated and, which is often written in terms of the respective eigenvalues λ_i and eigenvectors ϕ_i, where the first D values are those dimensions which span the signal subspace and all remaining values span the noise subspace [56].

Popular subspace techniques to estimate the DOA for narrowband signals are MUlltiple SIgnal Classification (MUSIC) and Estimation of Signal Parameter via Rotational Invariance Technique (ESPRIT). There are several variants to these algorithms which extend usage for varied application but they each follow the base algorithm described herein.

MUSIC works by utilizing the estimated subspaces to determine a power estimate for all angles of interest. The signal subspace is defined by

$$\hat{U_S} = [\hat{\phi}_1, \hat{\phi}_2, \ldots, \hat{\phi}_D] \tag{2.11}$$

and the noise subspace defined by

$$\hat{U}_N = [\hat{\phi}_{D+1}, \hat{\phi}_{D+2}, \ldots, \hat{\phi}_N] \tag{2.12}$$

Approximating that there are D eigenvalues in the signal subspace, this estimation is computed via

$$\hat{Q}_{MU}(\psi) = v^H[I - \hat{U}_S\hat{U}_s^H]v(\psi) \tag{2.13}$$

where v is the array manifold, I is the identity matrix, and ψ are the angular estimates under investigation. H is indicative of the Hermitian operator. The DOA angles are defined by the peaks found from this estimate, for the number of signals estimated to be present by the subspace estimation step. MUSIC can easily be expanded for usage on arbitrary array geometries by expanding ψ to $[\psi_x\psi_y]^T$[56]. The computational complexity for this algorithm is not small and should be considered where there is a constraint for computational capacity.

In an effort to reduce the computation complexity of the MUSIC algorithm, Roy and Kailath proposed ESPRIT [45]. The ESPRIT algorithm relies on pairs or doublets of array elements to make an appropriate estimate. Thus, for low-element array geometries, this

method is not appropriate. However, for larger arrays with sufficient equipment capacity, the ESPRIT algorithm works by first knowing the two signals A_1 and A_2 for each pair of elements, where the elements for each subarray are accounted for by the selection matrices J_1 and J_2

$$A_1(\theta) = J_1 A(\theta) \tag{2.14}$$

and

$$A_2(\theta) = J_2 A(\theta). \tag{2.15}$$

The two received signals are related by Φ

$$A_2 = A_1 \Phi \tag{2.16}$$

where

$$\Phi = diag[e^{j(2\pi/\lambda)d_x sin(\theta_1)}, \ldots, e^{j(2\pi/\lambda)d_x sin(\theta_L)}] \tag{2.17}$$

There exists a matrix T such that the received signal A can be written in terms of the signal subspace U_s as in

$$A = U_s T \tag{2.18}$$

and the number of source signals is the number of columns in U_s [56].The signal subspace can be rewritten in terms of U_s for each subarray to be

$$U_{s1} \Psi = U_{s2} \tag{2.19}$$

where

$$\Psi = T\Phi T^{-1}. \tag{2.20}$$

Using a least squares estimate to minimize the difference between the received signals U_s, Ψ can be solved for, thus allowing for the solution of Φ which gives rise to the DOA estimates θ [56, 55]. ESPRIT is particularly suitable for uniform linear arrays, due to the reliance on the shift invariance between the sets of array elements [63].

2.6 Limitations

For arbitrary array geometries, the estimators currently implemented are considerably more limited as most of them rely on some sort of uniformly spaced arrays. Some uniform array geometries are subject to FOV limitations and side-of-the-array ambiguity, making them insufficient for DOA estimation over an entire FOV. Small-element arrays also limit the capabilities of the estimators [55].

Further, most estimators were designed for usage on narrowband signals. Due to the additional complexities introduced by wideband signal sources, many of these methods are not directly applicable. Rather, there are additional signal manipulations that must be done prior to usage of these narrowband methods such that the wideband signal is separated into its narrowband counterparts [56, 55].

Many estimators rely on number of source estimation prior to the actual DOA estimate. This value can be known a priori or can be computed by analyzing the data. Though methods exist to determine this parameter, they are often error prone [55]. Because most of the source number estimation techniques rely on strictly the eigenvalues of the correlation

matrix to make a determination, some applications for DOA, particularly that of a radar application where multiple targets exist in the same range bin, are prone to nonsensical results.

CHAPTER III

DOA ESTIMATION FOR CONFORMAL ARRAYS ON REAL-WORLD IMPULSIVE ACOUSTIC SIGNALS

3.1 Introduction

Direction of arrival (DOA) estimation of singular stationary, impulsive, acoustic sources via a single conformal microphone array is of current interest. DOA, as referenced in this chapter, refers to the azimuth angle at which the acoustic signal wave impinges on the array. The most common methods for DOA estimation were designed for use on narrowband signals against a uniformly-spaced array [62].

Primarily, sensor array geometries used for DOA application are one-dimensional uniform linear arrays (ULAs), though two-dimensional uniform rectangular arrays (URAs) and uniform circular arrays (UCAs) are also common [66]. Conformal arrays, or geometries that do not follow a uniform spacing pattern and particularly those which span three dimensions, are rarely studied and are underrepresented in the literature. Though the array used in this study follows a pyramid geometry, the non-uniform element spacing qualifies the setup as a conformal array [32].

Most popular DOA estimators were designed for usage on narrowband signals. Though methods which extend the narrowband estimators into wideband estimators via separation

of the signal into narrowband frequency bins have been proposed, few are done on conformal arrays and thus do not provide a sufficient solution.

The contributions of this chapter are:

1. Exploring plausible solutions for DOA estimation of wideband signals on an arbitrarily-spaced microphone array.

2. Studying the effects of array configuration manipulation on these solutions to determine if employing sets of uniformly-spaced sub-arrays can achieve comparable estimation.

3. Evaluating the efficacy of described methods on real-world, impulsive acoustic signals.

The contents of this chapter are as follows. Section 3.2 discusses the task of estimating the DOA of a singular, impulsive acoustic signal using a conformal microphone array, Section 3.3 outlines the methods which will be explored and compared in this publication, Section 3.4 details the preliminary test experiments, and Section 3.5 reviews the results. Finally, Section 3.6 provides conclusions and lists future work.

3.2 Background

The acoustic events of interest are expected to occur in an environment with a generally clear and quiet surrounding to minimize reverberation and interference. Because of the impracticality of knowing a priori the general angle of arrival, the estimator must be able

to determine an appropriate azimuth angle, given a 360° field of view. The array element positioning is assumed to be known and supplied to each estimator.

The microphone array geometry referenced in this research was developed to balance a cost-restricted minimum number of elements for optimum amount of performance and accuracy. The geometry follows a pyramid-like pattern, composed of five microphones with four base elements. Each opposite base element is $1.3m$ from one another and the apex of the array centered $1m$ above the cross-section of the lower elements, relative to the East-West axis. The North-South axis sits $0.1m$ above the East-West axis. The entire array is positioned $2m$ above the ground. This array geometry is shown in Fig. 3.1.

Figure 3.1: Five-microphone conformal array.

Given that the array is fixed and cannot be altered for this application, usage of methods created for other array geometries is limited; only methods which are not geometry-specific

were considered. It is expected that the uniformly-spaced sub-arrays of the defined conformal array can be exploited to extend the applicable methods. Because ULAs and UCAs are the most commonly used array geometries for DOA estimation, this property extends the available estimators.

Uniformly-spaced arrays, particularly uniform linear arrays, are the most commonly used array geometry configuration for DOA estimation because of their simplicity to implement and analyze. However, they are subject to symmetric ambiguity properties, where one cannot distinguish which side of the array the event occurred without prior knowledge and thus are limited to a 180° field of view [12]. UCAs, however, provide uniform performance for a full 360° field of view and are desirable for DOA because of this property [12].

Despite the prevalence of wideband signals in real-world applications, most estimators that have been designed for conformal array geometries are for narrowband signals and are not suitable for wideband signals because these estimators assume a carrier frequency that can be accurately aligned and precisely measured; this includes the widely-used MUSIC method and several beamforming techniques. Wideband signals span the frequency spectrum such that narrowband methods that exploit phase differences amongst elements cannot be directly used [56].

3.3 Methods

The methods discussed in this section were both designed for usage on wideband signals and employ the time difference of arrival (TDOA) measurements to derive an esti-

mation. The first method explored is the GCCEstimator from MATLAB's phased array toolbox (GCC). Its estimation outputs determine both the azimuth and elevation angles [35] and it assumes the source to exist in the far-field. The second method (ULS) derives an estimated source location and propagation speed simultaneously and assumes the source to exist in the near-field [6]. From the estimated source location, a DOA is geometrically estimated.

3.4 Experiments

Three experiments were conducted to highlight the effectiveness of GCC [35] and ULS [6] in estimating the angle of arrival. Section 3.4.1 shows the estimators' predictions for four cases of varied angles and distance about the array, Section 3.4.2 explores sub-array manipulation and its effects on the estimators, and Section 3.4.3 shows how the estimators respond to additional real-world, impulsive acoustic signals.

The directionality described throughout experimentation is relative to the definition of the array geometry. For consistency amongst experiments, the array is positioned such that the four base elements exist at the cardinal directions, if one were to aerially view the array. The directionality is defined such that East corresponds to $0°$, North corresponds to $90°$, West corresponds to $\pm 180°$, and South corresponds to $-90°$.

For the purposes of this set of experiments, there is assumed to be some error in the initial measurements, and thus the expected values are denoted by $\approx \theta$, where $\approx$ indicates an approximation. For the case of GCC, the propagation speed of the acoustic signals is the standard $343 m/s$. This parameter varies with the temperature and humidity of the

propagation medium and is likely offset due to the environment the tests were performed in. Furthermore, the angular measurements were obtained via rudimentary instrumentation. Approximate estimations are sufficient to determine efficacy.

The conformal microphone array is composed of five omnidirectional microphones that are simultaneously sampled at $40kHz$. Each acoustic event sample is characterized by a $6s$ window where the onset of the acoustic event is centered at $3s$. The GPS clock onboard the array has an accuracy of $\pm 200ns$. The sample size for each collected acoustic event is $240,000$ data points. The entire span of the event was considered in comparison calculations.

3.4.1 General Accuracy

To simulate the expected impulsive, wideband event, a series of four tests were conducted, where M-150 fireworks were set off at differing distances and azimuth angles with respect to the center of the microphone array, as shown in Fig. 3.2. Using all five channels of the data to compute the estimate, the angles of arrival were computed.

3.4.2 Altered Array Configuration

Due to the low number of elements restriction of the array, there are limited subconfigurations that it can be split into. The most inclusive case, detailed in Section 3.4.1, utilizes all five elements of the array. The second set most desirable geometry that can be created from the base array is a UCA or URA. Because the base is composed of four elements, the geometry is the same for these configurations and is treated as such. Because triangular geometries are not seen in the literature and because the triangular subsets are

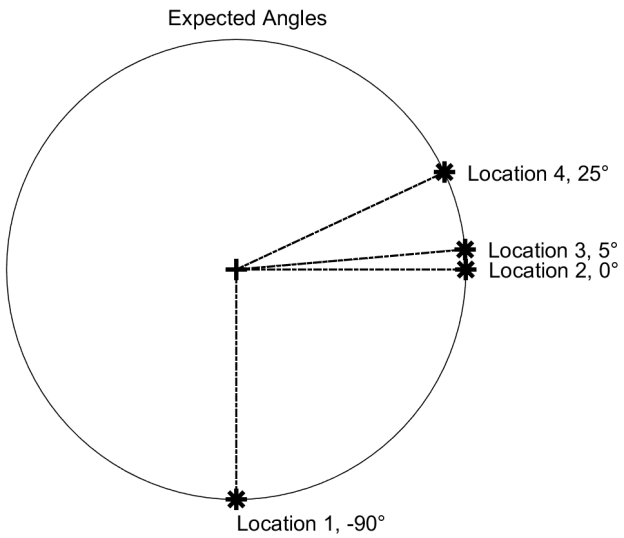

Figure 3.2: Expected source locations for general accuracy experiment.

not uniformly spaced, three-element configurations were not considered. The smallest and most fundamental subsets of the array geometry are those ULAs formed between all sets of pairs.

Given the element labeling in the array configuration shown Fig. 3.3, the sub-arrays described in Table 3.1 can be created.

Using the same dataset as the experiment in Section 3.4.1, each sub-array was used to determine the DOA.

3.4.3 Other Acoustic Sources

Two additional sets of impulsive acoustic signals were generated by striking two scraps of lumber and using a standard marine airhorn to evaluate how the estimators handled proximity and source variance.

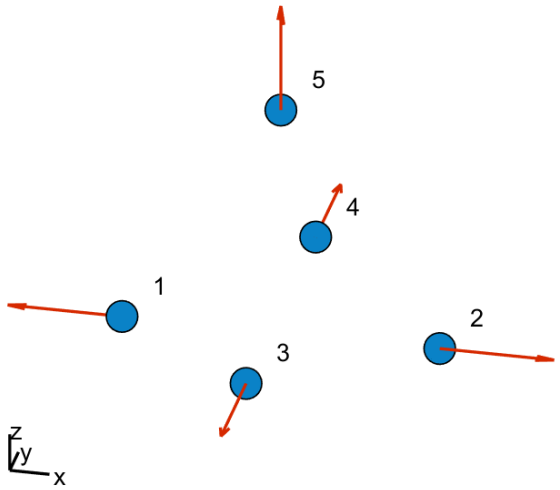

Figure 3.3: Labeled array elements for sub-array extraction.

Table 3.1: Sub-Array Configurations

Array Geo.	**Num. Elem.**	**Elem. Labels**
Conformal Arr.	5	1, 2, 3, 4,5
URA/UCA	4	1, 2, 3, 4
ULA (Opp. Ang.)	2	1, 2
ULA (Opp. Ang.)	2	3, 4
ULA (Adj. Ang.)	2	1, 3
ULA (Adj. Ang.)	2	1, 4
ULA (Adj. Ang.)	2	2, 3
ULA (Adj. Ang.)	2	2, 4
Angled ULA	2	1, 5
Angled ULA	2	2, 5
Angled ULA	2	3, 5
Angled ULA	2	4, 5

The claps were generated near the perimeter of the array at $\approx 1m$ from the array, while the airhorn was blown $\approx 50m$ away. The general directionality was noted for each event and thus approximate accuracy can be compared. The expected regions of interest (ROI)

for each acoustic event are detailed in Table 3.2 and Table 3.3 and graphically shown in Fig. 3.4.

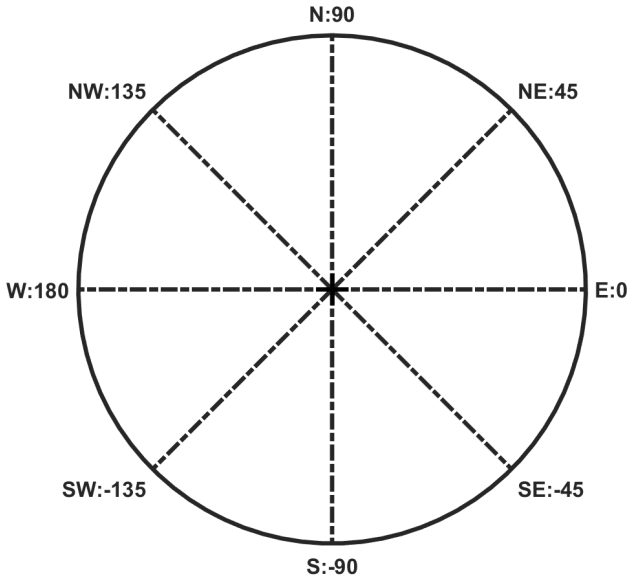

Figure 3.4: Regions of interest with respect to the array, aerial view.

3.5 Results and Discussion

Although the methods compared both utilize the TDOA information to compute the DOA, some variance in the initial estimation results exists.

3.5.1 General Accuracy Results

GCC estimates the direction, where the ULS approach estimates a definitive location that can be geometrically interpreted into an angle of arrival. Based on the results in Table 3.4 and the plot in Fig. 3.5. the geometric angle estimation from the estimated position for ULS seems plausible, despite some discrepancies in the expected values for computed

Table 3.2: Acoustic Source ROI- Lumber.

Direction	**Region**
Northwest	$90°$:$180°$
Southwest	$-90°$:$-180°$
South	$-45°$:$-135°$
Southeast	$0°$:$-90°$
East	$-45°$:$45°$
Northeast	$0°$:$90°$

Table 3.3: Acoustic Source ROI- Airhorn.

Direction	**Region**
North	$45°$:$135°$
Northwest	$90°$:$180°$
West	$-135°$:$135°$
Southwest	$-90°$:$-180°$
South	$-45°$:$-135°$
Northeast	$0°$:$90°$

distance. Note that red-colored estimates correspond to GCC and blue-colored estimates correspond to ULS.

For three of the four test locations (2, 3, and 4), both methods compute the DOA to nearly or exactly the same value, of which are appropriate for the expected values. However, the ULS method incorrectly estimated the angle for the location 1 and instead estimated an angle nearly $180°$ off, highlighted in Table 3.4.

3.5.2 Altered Array Configuration Results

From the sub-array configuration experiments, it was shown that as element reduction occurred, performance decreased significantly. The uniformity of the base of the conformal array provides adequate resolution for $360°$ azimuth angles, and thus performs well in the four-element case. However, the sparsity of most of the two-element sub-arrays is not

Table 3.4: DOA Estimations for General Accuracy.

Loc.	**GCC**	**ULS**	**Expected**
1	$-91°$	$89°$	$\approx -90°$
2	$1°$	$1°$	$\approx 0°$
3	$4°$	$4°$	$\approx 5°$
4	$21°$	$20°$	$\approx 25°$

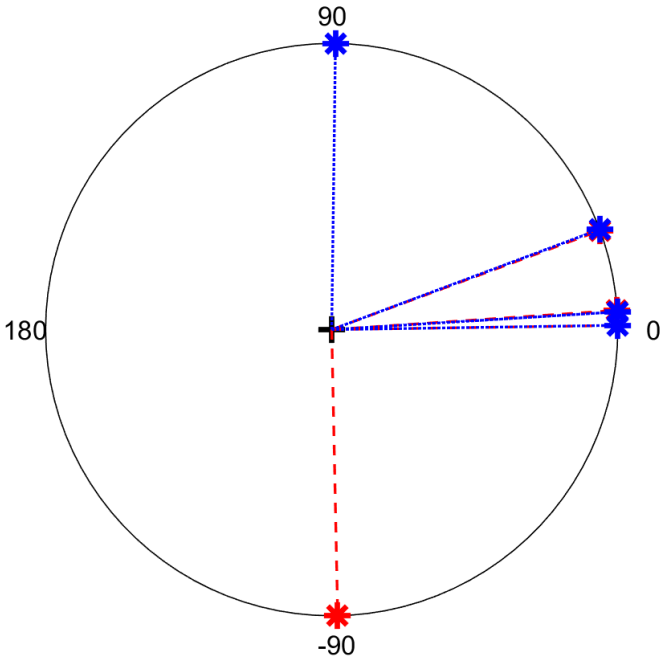

Figure 3.5: Estimated angles of arrival relative to the array.

sufficient enough to estimate a proper direction of arrival. ULS was unable to derive a solution for any of the two-element sub-arrays and thus the results for these experiments are not included. The DOA estimates for MATLAB's GCC are shown in Table 3.5.

This experiment suggests sub-arrays may be employed with methods which require ULA and UCA geometries.

Table 3.5: DOA estimations on sub-array geometries defined in Table 3.1.

Array Configuration	**Loc. 1**	**Loc. 2**	**Loc. 3**	**Loc. 4**
1,2,3,4,5 - Expected	$\approx -90°$	$\approx 0°$	$\approx 5°$	$\approx 25°$
1,2,3,4,5 - Actual	$-91°$	$1°$	$4°$	$21°$
1,2,3,4	$-91°$	$1°$	$4°$	$20°$
1,2	$-180°$	$0°$	$0°$	$0°$
3,4	$-68°$	$1°$	$3°$	$20°$
1,3	$-45°$	$-45°$	$-45°$	$-45°$
1,4	$-135°$	$45°$	$45°$	$45°$
2,3	$-135°$	$45°$	$45°$	$45°$
2,4	$-45°$	$-45°$	$-45°$	$-45°$
1,5	$180°$	$0°$	$0°$	$0°$
2,5	$0°$	$0°$	$0°$	$0°$
3,5	$-34°$	$-6°$	$0°$	$7°$
4,5	$-12°$	$7°$	$2°$	$6°$

3.5.3 Additional Acoustic Source Results

Based on the primitive tests for this set of experiments, acoustic sources sufficiently separated from the array are estimated in the correct general region, as shown in Table 3.6 and Table 3.7. Acoustic events occurring too near the array are subject to error. This is most likely due to the wavefront not being planar, as expected by the DOA estimators.

Table 3.6: Additional Source Estimations- Lumber.

Expected Region	GCC	ULS
≈90°:180°	130°	−46°
≈−90°:−180°	−145°	−128°
≈−45°:−135°	−92°	−85°
≈0°:−90°	−42°	158°
≈−45°:45°	3°	2°
≈0°:90°	51°	21°

Table 3.7: Additional Source Estimations- Airhorn.

Expected Region	GCC	ULS
≈45°:135°	90°	91°
≈90°:180°	124°	125°
≈−135°:135°	177°	177°
≈−90°:−180°	−144°	−127°
≈−45°:−135°	−92°	−94°
≈0°:90°	52°	52°

3.6 Conclusions and Future Work

The literature for DOA estimators that work on both impulsive acoustic sources and conformal array geometries is highly limited. Though there exist several techniques which sufficiently estimate a subset of these constraints i.e. narrowband signals with conformal arrays or wideband signals with uniform arrays, the solutions available which accomplish the task at hand with minimal computational complexity are scarce.

Utilizing GCC and its variants is an appropriate solution to determine the DOA of a single wideband source. These methods are limited by the ability to localize a single source.

Examining uniform subsets of the defined conformal array suggests that estimators designed for these uniform configurations may be plausible options. With each subset

configuration, it was noted that accuracy decreased as elements were omitted. Ideally, there would be more elements, but because of the constraint of the equipment, this is not an option. Wideband methods which operate on the URA, UCA, and ULA sub-configurations to explore include the methods referenced in [40].

Other wideband methods for conformal arrays of interest to explore are IMUSIC for its desirable properties on high SNR data, and TOPS for its unique subspace processing [46].

Narrowband methods that have been extended for use on wideband signals by partitioning the wideband signals into their narrowband counterparts and averaging the results from each frequency bin to approximate a wideband solution have been shown to reveal promising results and thus should also be explored in future works [56].

Ultimately, the directionality of multiple events of this nature and of which may also be non-stationary will be of interest. Pham and Sadler proposes a method (AMI-UCA MUSIC) which is able to accomplish this on a UCA [42]. The method proposed in [61] can distinguish multiple sources more precisely than IMUSIC. Because of the possible sub-array extension, the approach may be appropriate.

CHAPTER IV

ROBUST ESTIMATION OF THE NUMBER OF RADAR SIGNAL SOURCES USING DEEP LEARNING

4.1 Abstract

This chapter presents a deep-learning based approach to estimating the number of sources in radar. This is an important problem in radar, sonar and communication systems, as many angle–of–arrival estimators require accurate estimates of the number of sources. Herein, a robust method that performs well when all targets are in the same range bin is developed. The standard estimators which base estimates on the number of large eigenvalues of the covariance matrix, such as the Akike Information Criteria (AIC), Minimum Description Length (MDL) estimator, and MUltiple SIgnal Classification (MUSIC) all fail when the targets are in the same range bin and are all illuminated by the same pulse, so that the target information is mostly contained in the largest eigenvalue. The proposed method is compared to the Minimum Variance Distortionless Response (MVDR) spectral estimator, and the proposed method shows superior performance.

4.2 Introduction

Estimating the number of plane wave sources is an important problem in fields such as radar, sonar, and communication systems. Traditional approaches often rely on the eigen-

values of the covariance matrix, which limits their performance. These methods will fail in the case where there are multiple targets at the same range bin, because the returns will all be grouped into one eigenvalue. This paper introduces a deep-learning-based method that utilizes the covariance information in addition to the eigenvalues to accurately estimate the number of sources. The proposed method achieves excellent results, and works in situations where typical methods such as the Akike Information Criteria (AIC) estimator, Minimum Description Length (MDL) estimator, MUltiple Signal Classification (MUSIC), and Minimum Variance Distortionless Response (MVDR) fail. To the best of our knowledge, this is the first deep learning network applied to the fusion of covariance data and eigenvalues used to analyze the number of incoming target signals. Specifically, the contributions of this chapter are:

1. A robust deep learning system that achieves state-of-the-art results and far surpasses traditional eigenvalue-based methods, which fail in the scenarios examined herein.

2. Fusion of the covariance matrix and the eigenvalues for joint analysis, which provides the best results.

3. This algorithm works even when the number of receivers and number of pulses in a coherent processing interval are small.

The contents of this paper are as follows. Sec. 4.3 discusses background information. Sec. 4.4 outlines the proposed method. Sec. 4.5 details our datasets, and sec. 4.6 discusses our results. Finally, sec. 4.7 provides conclusions and lists future work.

4.3 Background

4.3.1 Previous Work

The novel work presented in this study was influenced by findings in prior development of a source number estimation technique for radar signals. The development of a neural network (NN) based on Radial Basis Function (RBF) was expected to perform more accurately than other current methods, due to the neural networks ability to adapt to the data. For this study, simulated radar data was created based on the signal model defined in [59]

$$x(t) = \sum_{i=1}^{q} A(\phi_i) s_i(t) + n(t), \tag{4.1}$$

where $A(\phi_i)$ is a transformation which projects the signal across the array of receivers, s_i is the raw signal, and $n(t)$ is the noise.

This RBFNN was designed to accept the eigenvalues as inputs to the network, such that the network could be compared to other methods that rely on eigenspace decomoposition. The eiegenvalues were extracted from the simulated data, which was designed such that 0-3 targets existed in the same range bin, for various test cases.

DOA estimation in radar signal processing occurs individually for each range bin containing detections. Because range-based detections do not indicate the number of targets in individual range bins, the number of sources in a single range bin must be estimated for many DOA algorithms. Because of the nature of multiple targets existing in the same range bin, the signals do not behave as desired when performing eigenanalysis, which is typically used as the preferred method to estimate the number of sources. Each target signal is a reflection of the transmitted pulse with a phase ramp across the receivers, relative

to differences in distance from the target to each receiver. Signals in the same range bin are aligned in phase if the effect of the phase ramp is not considered. Because the receivers in radar systems have very small element spacing, the phase ramp on the signal is similarly small. Thus, signals reflected by each target differ marginally from one another and act as one signal- the equivalent of two sinusoids equal in phase and frequency. When eigenanalysis is performed on the simulated data, the signals for each target do not associate with separate eigenvalues. Instead, the largest eigenvalue is approximately the sum of the power of all signals and the noise variance.

After testing the RBFNN with the specific variants of radar data, it was then discovered that strictly-eigenvalue-based methods are insufficient to find the number of targets in a single radar range bin. As such, the motivation to design an approach to estimate the number of targets that does not solely rely on eigenvalue analysis was begun.

4.3.2 Nomenclature

Table 4.1 gives the mathematical symbols used herein.

4.3.3 Conventional source estimation methods

In radar signal processing, estimating the number of signals present in noisy data is a complex problem that has been extensively studied. It is often advantageous for the radar to know how many sources are present in a signal, in order to facilitate better target detection and tracking. Many angle of arrival (AOA) estimation algorithms such as MUltiple SIgnal Classification (MUSIC) [49], Estimation of Signal Parameters by Rotational Invariance Techniques (ESPRIT) [45], and the Maximum Likelihood Estimator (MLE) (especially

Table 4.1: Mathematical Symbols and Notations

Variable	Description
$\mathbf{x}_m$	Receive data vector for m-th pulse
$\mathbf{X}$	Receive data matrix
$\mathbf{R}_{XX}$	Covariance matrix
$\mathbf{R}_{XX}(m,n)$	Covariance matrix m,n entry
λ_i	Covariance matrix i-th eigenvalue
K	Number of rows and columns in covariance matrix
P	Number of pulses (independent realizations)
M	Number of receiver channels
T	True number of targets present
$\hat{T}$	Estimated number of targets present
Δx	Array element spacing (meters)
ϕ_k	Azimuth angle of k-th target
n_m	Noise in the m-th receive channel
N	Number of azimuth angles in MVDR FOV sweep
δ	Diagonal loading for MVDR

the efficient implementation [65]) have been proposed to address this problem. These techniques are called superresolution techniques because they can localize more accurately than the Rayleigh Resolution [56].

However, MLE requires prior estimates of the number of sources. MUSIC, like MLE, has to make a parameter sweep, and its computational complexity grows exponentially with dimension. Moreover, these superresolution techniques require extensive computations and are generally not suitable for real-time implementation [17]. Furthermore, algorithms like MUSIC and ESPRIT can become unstable when the number of receiver channels are small [33]. MUSIC is also susceptible to poor performance when the source signals are coherent [36, 41], which is the case in this paper.

The MVDR algorithm is both a beamformer and a superresolution AOA estimator. The MVDR can be utilized to both estimate angles of arrival and to estimate the number of sources, as long as the sources are separated adequately. Using MVDR as a AOA estimator or a number of sources estimator requires a parameter sweep across the radar's field of view (FOV). The MVDR response with a diagonal load added to the signal covariance matrix [56] is

$$MVDR\left(\theta\right) = \frac{1}{\mathbf{v}^{H}\left(\theta\right)\left(\mathbf{R}_{XX} + \delta\mathbf{I}\right)^{-1}\mathbf{v}\left(\theta\right)} \tag{4.2}$$

where δ is a small positive diagonal loading constant, which is used to help poorly-conditioned covariance matrices; θ is an azimuth angle that takes on values $\theta \in \{\theta_1, \theta_2, \cdots, \theta_N\}$, where N are the number of points in the FOV sweep; and $\mathbf{v}\left(\theta\right)$ is the array manifold vector for the steering angle θ [56]. Moreover, it is still an open problem in radar to determine the optimal diagonal loading parameter. This is typically done empirically. The N theta values for the FOV are called the pseudo-spectrum. The pseudo-spectrum is evaluated by utilizing a peak finding algorithm. The system must set some threshold for peaks, since noise with no targets can also cause peaks in the MVDR pseudo-spectrum. The peak locations give information about the signal strength and the target AOA relative to the radar.

Two disadvantages of this approach are that the numerator requires a $[1 \times M]$ by $[M \times M]$ by $[M \times 1]$ matrix multiplication and a division for each azimuth value in the FOV sweep, and a matrix inverse operation is required. The $[M \times M]$ matrix inverse can be pre-computed prior to the FOV sweep loop and can be implemented using Lower-Upper

(LU) decomposition, singular value decomposition, Cholesky decomposition, or QR decomposition [2]. Because a matrix inverse is required, enough data samples must be available or the inversion will be inaccurate (or a larger diagonal load will be required, which will reduce the MVDR sensitivity).

Arguably the most common method for estimating the number of signals is the AIC [4]. Rissanen points out that the AIC yields inconsistent estimates, and in radar, often overestimates the number of signals [44]. To eliminate this behavior, he developed the MDL estimator. However, the MDL can underestimate the signal subspace, especially when the samples are small [43]. Both AIC and MDL utilize the covariance eigenvalues to estimate the data dimensionality. Radoi et al. [43] utilized analysis of the covariance matrix eigenvalues to more accurately estimate the number of signals present. They developed a discriminant function that estimates both the dimensionality of the signal and noise subspaces, and combine these two discriminants into one estimator.

The covariance matrix eigenvalues are a complicated function of the signal strength, distance between the signals, and the relative locations of the signals. The lower-valued eigenvalues are generally associated with the noise, at least for high signal-to-noise ratios (SNRs). With lower SNRs, the noise eigenvalues start taking on higher and higher levels, and will eventually become virtually indistinguishable from the eigenvalues associated with the signal subspace. Methods that only use the eigenvalues as inputs lose a significant amount of signal information. There is another major issues with these methods when the number of receiver channels is small: the receive array has a large Rayleigh resolution [56], and multiple sources tend to blend together. The eigenvalue-based methods break

down in these cases. Moreover, when there is one signal transmitted and the targets are in the same range bin, the return information is mostly contained in the first eigenvalue of the covariance matrix. Therefore, these eigenvalue-based methods will fail in this case, and alternate methods are needed.

4.3.4 Shallow Neural Networks

Neural networks (NNs) are loosely meant to mimic neurons in the brain. In a typical shallow NN, each neuron has a number of inputs which are multiplied by weights and a bias term is added to this sum. Then the activation function is usually a non-linear function of the weighted inputs plus the bias. Multiple layers allows the NN to learn any complex function of the inputs, provided enough neurons are present and there are at least two layers [13]. NN are typically trained by backpropagation, which adjusts each weight in the network according to the error criterion in the training function. Many authors have developed NN approaches to AOA estimation in radar [30, 38, 60, 52, **?**, 18, 17, 50, 8, 47, 48, 10, 31, 64, 58, 19, 33, 23, 41, 37, 3]. However, to the best of our knowledge, no one has published a NN to estimate the number of sources. Herein, we briefly review some of these papers.

El Zoohgby et al. in Ref. [16] utilized the covariance matrix and a radial basis function (RBF) NN to estimate the angles of arrival of multiple radar signals. The covariance matrix contains detailed information about the incoming data signals. Du et al. [14] examines several NN architectures for antenna array signal processing: multilayer perceptrons, Hopfield networks, radial-basis function NN (RBFNN), PCA-based NN, and Fuzzy NN. It

is relatively straightforward to implement a Hopfield network in hardware, and the fuzzy NN can achieve faster convergence with a smaller network size.

Amari and Cichocki [5] examine adaptive blind signal processing using NN, with one goal for the algorithm to work when the number of sources is unknown. They employed a fully-connected recurrent NN and provided a list of ten open questions in the field. Several papers noted that RBFNN outperforms MUSIC in accuracy and speed [8, 16, 15]. El Zooghby [17] utilized a RBFNN for multiple source tracking in a smart antenna application. Lo et al. used a RBFNN for AOA estimation and found it performed better than MUSIC [38]. Tan et al. utilize a RBFNN to approximate an inverse function of the nonlinear mixing mapping and developed a contrast function to embed inside a RBFNN [54]. Solazzi et al. [51] developed a spline NN to address blind source separation. They utilized this network to analyze speech data. All of these networks are not appropriate for radar data because the data is complex. Complex NN have been studied for about 15 years now [25, 26], but there is little published on radar processing using a complex NN.

Matsuoka et al. [39] put forth a NN and a learning algorithm for blind separation of nonstationary signals. Kim and Ling utilized a network with multiple steered beams to generate features used to track humans [33]. They first perform digital beamforming to generate 12 beams, and the AOA estimation utilizes the beam return power as a feature vector for a multi-beam monopulse method. Ofek et al. designed a 2D AOA RBFNN estimator by restricting subnetworks to small sectors, then performing analysis in the sectors [41].

Agatonovic et al. [3] designed a NN to estimate azimuth and elevation AOA for a 2D space division multiple access communications array. The NN can learn and account for array mutual coupling and measurement imperfections to some extent when trained with measured data. Chang et al. implemented a NN MVDR beamformer using a Hopfield-type NN [11]. They converted the complex-valued constrained MVDR quadratic programming problem into a real-valued problem which the NN can handle.

Shieh and Lin [50] wanted a lower cost (computationally) solution to AOA estimation than MUSIC and MLE. They developed a self-constructing neural fuzzy inference network (SONFIN), which automatically determines an economical network size. The network uses sets of phase differences as inputs, and the internal nodes implement a fuzzy logic system. Their system estimates one AOA, and is not suitable for multi-AOA problems.

Southall et al. utilize a multi-layer RBFNN to estimate AOA for one target [52]. The proposed algorithm performed better than a competing NN. This system is limited to estimating one AOA.

4.3.5 Deep learning

Deep learning has gained much attention in the research communities due to significant performance gains of many deep learning systems over more standard (hand-crafted) feature systems (the so-called "shallow" systems). Although there is no hard-and-fast rule for what constitutes a shallow versus a deep network, most researchers would agree networks of 5–10 or more layers are considered deep. Deep networks can learn very complicated features and decision boundaries from the training data, and can also learn hierarchical fea-

tures. Deep networks are typically composed of many thin (not tall) layers, while standard shallow neural networks are usually composed of few layers, and each layer can be very tall (have a large number of neurons).

Shallow neural nets (of at least depth two), if given enough neurons, can approximate any function to any desired accuracy [13]. Deep networks can also approximate any function, but they don't generally require networks that are as tall as a shallow network would have to be.

Grais et al. utilized a deep (five layer) NN where the initial estimates were generated using non-negative matrix factorization. Their system identified the data source (source one or source two) in speech processing [22]. Vesperini et al. put forth a deep learning system that could handle multiple rooms and static and moving sound sources [57]. Although these are not applications with radar signals, they do show that a deep learning system can perform AOA analysis.

4.4 Proposed Method

The proposed method utilizes a deep NN whose inputs are the real and imaginary portions of the covariance estimate, as well as the covariance eigenvalues. The network optimally fuses these inputs to provide a robust solution to estimating the number of input signals. To the best of our knowledge, this research is the first to apply a deep NN to analyze of the number of radar signals.

4.4.1 Signal Model

Herein, the following complex–valued radar signal model is utilized:

$$x_m = \left[\sum_{k=1}^{T} a_k \exp\left(-j2\pi \frac{f}{c} \Delta x \, m \sin\left(\phi_k\right) \right) \right] + n_m \tag{4.3}$$

where $j = \sqrt{-1}$, x_m is the complex received signal at the m–th receiver, T is the number of sources, a_k is the amplitude of the k–th source, ϕ_k is the azimuth angle of the k–th source (in radians), Δx is the element spacing in meters, f is the radar frequency in Hz, c is the speed of light in meters/second, and n_m is IID complex white Gaussian noise associated with the m–th receive channel (and is independent across channels). When there are no sources, the summation will have value zero. The radar collects P pulses. The data from pulse p is stored in the $[K \times 1]$ complex vector $\mathbf{x}_p = [x_1, x_2, \cdots, x_K]^T$ and the data from all P pulses is stored in the $[K \times P]$ receiver data matrix $\mathbf{X} = [\mathbf{x}_1, \mathbf{x}_2, \cdots, \mathbf{x}_p]$. The targets are Swerling 1 targets, with signal-to-noise ratios (SNRs) ranging from -10 to 20 dB.

4.4.2 Radar parameters

The radar is a notional uniform linear array operating at $f = 5.0$ GHz with element spacing $\Delta x = \lambda/2$. There are $M = 10$ receivers in the array, and this value was chosen to present a small array (in order to challenge the algorithms). The number of pulses per coherent processing interval is $P = 10$, which was also chosen to be a smaller number of pulses in order to evaluate the proposed method with a smaller number of pulses.

4.4.3 Proposed deep learning network

Herein, a deep learning method is utilized which requires very few neurons and provides robust results. For a 10-channel receiver, there will be 210 inputs to the network.

The network consists of three sets of fully-connected layers followed by the parametric rectified linear units (PReLUs) [24] and batch normalization layers. Then a dropout layer is inserted to help mitigate overfitting. Next, there is another set of fully-connected layers followed by PReLU and a batch normalization layer, followed by softmax and classifier layers. The deep learning architecture is described in table 4.2 below.

Table 4.2: Proposed deep network architectures. NW 1 is the proposed network.

Layer	**Type**	**Size**
1	FC	210
2	PReLU	210
3	BN	210
4	FC	210
5	PReLU	210
6	BN	210
7	FC	210
8	PReLU	210
9	BN	210
10	DR	50%
11	FC	4
12	PReLU	4
13	BN	4

Table 4.2: (continued)

Layer	Type	Size
14	SM	4
15	CL	1

Note: FC = Fully Connected, PReLU = Parametric ReLU, BN = Batch Normalization, DR = Dropout, SM = Softmax, CL = Classifier, NW = Network.

By utilizing the PReLU, performance is increased over a standard rectified linear unit (ReLU). The PReLU allows information to flow from when the input is negative, whereas a Rectified Linear Unit (ReLU) does not. The PReLU has the following transfer function

$$f(x) = \begin{cases} x & x \geq 0 \\ & \\ -\alpha x & x < 0 \end{cases}, \tag{4.4}$$

where α is a parameter learned by the network. It allows negative activations to pass, whereas a standard ReLU kills any negative input by forcing it to zero.

The fully connected layers compute a dot product of the input values with the neuron weights and add a bias term. The weights are randomly initialized as zero-mean Gaussians with variance 0.01 and the biases are initialized as zero. The batch normalization layers provide a means to normalize the data (force the distribution towards a zero mean, unit variance Gaussian) in order to allow the network to be deep [28]. The softmax layer in conjunction with the classification layer learns a distribution to estimate the number of

sources [9]. All layer coefficient weights are learned using stochastic gradient descent with momentum [9].

4.4.4 Data analysis

In order to estimate the number of sources, a combination of the estimates of the covariance matrix itself and the covariance matrix eigenvalues is used herein. For each case analyzed, the $[K \times K]$ covariance data matrix is estimated using

$$\mathbf{R}_{XX} = \frac{1}{M}\mathbf{X}\mathbf{X}^{H}, \tag{4.5}$$

where the superscript H represent the Hermitian matrix transpose operator and $\mathbf{X}$ is the $[K \times P]$ receiver data matrix. Several possibilities for inputs to the proposed system were examined: (1) covariance matrix (split into real and imaginary portions), (2) eigenvalues of covariance matrix, (3) covariance matrix (split into real and imaginary portions) plus eigenvalues.

Figures 4.1, 4.2, and 4.3 show PDFs of the first three eigenvalues (where the eigenvalues are sorted in descending order) for zero, one, two and three targets, respectively. From figure 4.1 and 4.2, it is clear that the first eigenvalue contains a mixture of all of the targets plus noise. The second eigenvalue has some separability from the one, two and three target cases. It is noted that there is not clear indication of how many targets are present from eigenvalues 2 or 3. This is why methods such as AIC, MDL, etc. that depend on the eigenvalues will be useless in these cases and unable to estimate the number of reflections.

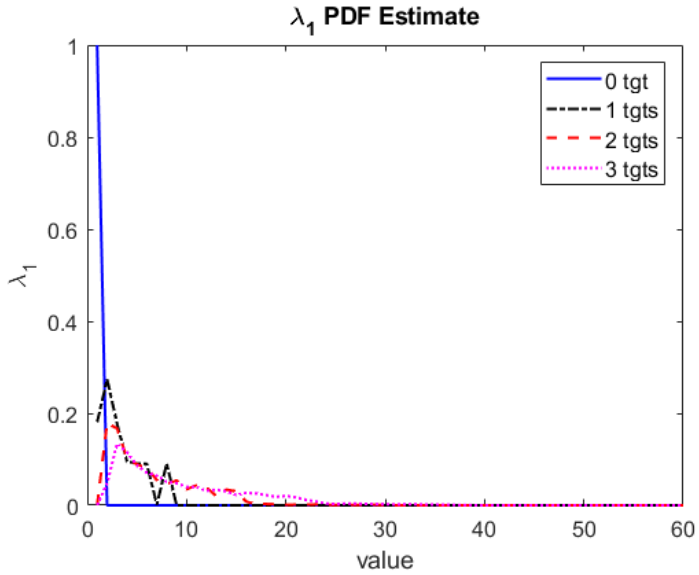

Figure 4.1: Eigenvalue PDF plot of first eigenvalue.

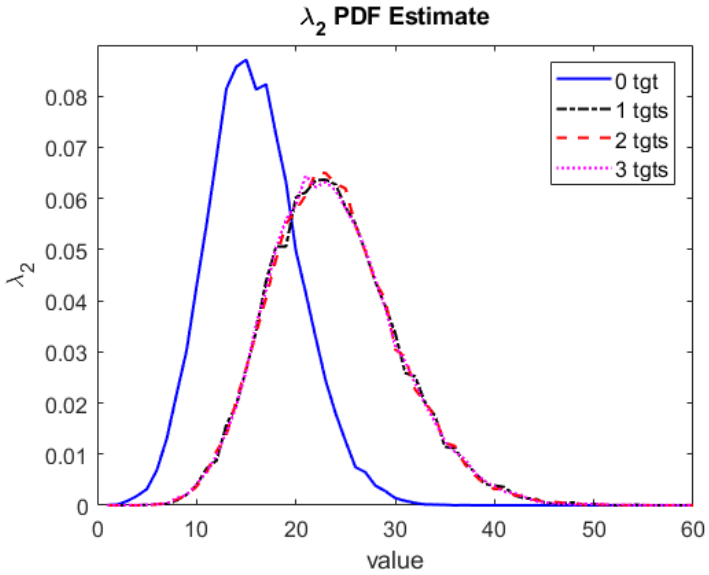

Figure 4.2: Eigenvalue PDF plot of second eigenvalue.

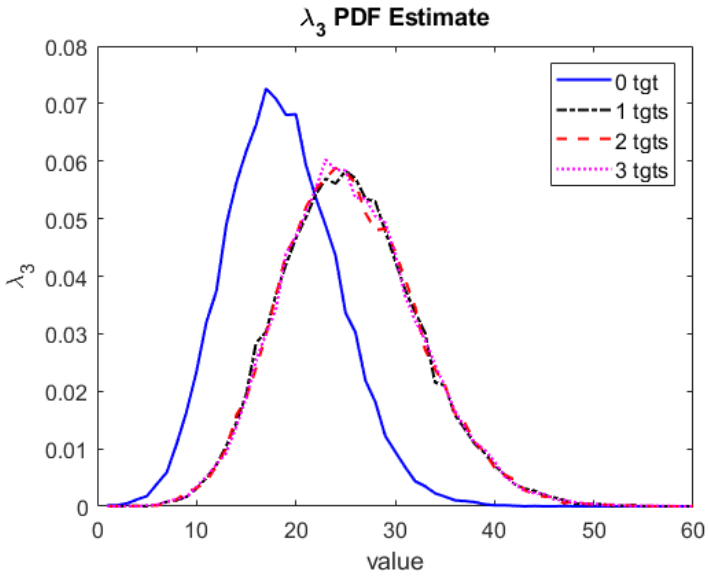

Figure 4.3: Eigenvalue PDF plot of third eigenvalue.

Herein, the covariance matrix is unrolled to produce a $[2K^2 \times 1]$ feature vector as follows:

$$\mathbf{f}_R = \begin{bmatrix} real\left\{\mathbf{R}_{XX}\left(1,1\right)\right\} \\ real\left\{\mathbf{R}_{XX}\left(2,1\right)\right\} \\ \vdots \\ real\left\{\mathbf{R}_{XX}\left(K,1\right)\right\} \\ \vdots \\ real\left\{\mathbf{R}_{XX}\left(K,K\right)\right\} \\ imag\left\{\mathbf{R}_{XX}\left(1,1\right)\right\} \\ imag\left\{\mathbf{R}_{XX}\left(2,1\right)\right\} \\ \vdots \\ imag\left\{\mathbf{R}_{XX}\left(K,1\right)\right\} \\ \vdots \\ imag\left\{\mathbf{R}_{XX}\left(K,K\right)\right\} \end{bmatrix} \tag{4.6}$$

.

Note that rounding errors and using a finite number of samples can cause the covariance matrix estimate to have small imaginary entries. The eigenvalues are computed using the Singular Value Decomposition (SVD) [7] as follows from the covariance matrix:

$$\mathbf{R}_{XX} = \mathbf{USU}^H, \tag{4.7}$$

where $\mathbf{S}$ is the diagonal singular–value matrix whose diagonals are the covariance matrix eigenvalues: $\mathbf{S} = diag\left(\lambda_1, \lambda_2, \cdots, \lambda_K\right)$, where $\lambda_1 \geq \lambda_2 \geq \cdots \geq \lambda_K$. The eigenvalue features are placed in the $[K \times 1]$ feature vector as follows

$$\mathbf{f}_\lambda = [\lambda_1, \lambda_2, \cdots, \lambda_K]^T. \tag{4.8}$$

The final data feature is the $[(2K^2 + K) \times 1]$ vector given by

$$\mathbf{f} = \begin{bmatrix} \mathbf{f}_R \\ \\ \mathbf{f}_\lambda \end{bmatrix}. \tag{4.9}$$

4.4.5 Proposed algorithm description

The proposed algorithm, shown below in Algorithm 1, uses the complex $[M \times P]$ receiver data matrix and estimates the number of sources present. This algorithm is designed for the hard case of potential multiple targets in one range bin.

4.5 Data sets

Simulated data are utilized to test the proposed method and to compare to traditional methods. Table 4.3 shows the various test cases utilized. In Table 4.3, $rand\left[A, B\right]$ means random values are selected in the range $A \leq x \leq B$ and $A : B$ means all integer values are selected from $\{A, A+1, \cdots, B\}$. In Table reftable:Experiments, the SNR values are per–pulse values.

ALGORITHM 1
Estimate number of targets.

Input: $\mathbf{X}$, $[M \times P]$ receiver complex data matrix.
Output: $\hat{T}$, estimate of number of sources.
Extract feature vector :
1: Compute the covariance matrix using eq. 4.5.
2: Compute eigenvalues using 4.7.
3: Compute the covariance feature vector using eq. 4.6.
4: Compute the eigenvalue feature using eq. 4.8.
5: Create the final feature vector using eq. 4.9.
Estimate the number of sources :
6: Evaluate feature vector with network.
7: **return** $\hat{T}$

In each test case, there are zero to three targets present. For no targets present, the signal is IID complex white Gaussian noise. When there is one or more signals present, the target angles are randomly selected using a uniform PDF covering the radar's FOV. For this work, FOV ranges from -60° to 60°. When multiple targets are present, any two targets are restricted to not to be closer to each other than $\Delta\phi = 0.5^\circ$, since the radar would not be able to distinguish target this close together. The target signals are added to the receiver noise, which is IID complex white Gaussian noise.

Test case 1 has all targets at 10 dB SNR. Taking test case 2 as an example, for training, there are 20,000 cases for no targets, 20,000 cases for one target, 20,000 cases for two targets, and 20,000 cases for three targets, for a total of 80,000 cases. For those training cases with at least one target, the the first target will have 10 dB SNR, and when there are multiple targets, the target SNRs are randomly chosen from 0 to 20 dB SNR. This is designed to see if the proposed method can handle a large dynamic range.

Test case 3 trains all targets at 5 dB SNR, and in testing, multiple targets are randomly chosen from 0 to 20 dB SNR. Test case 4 trains and tests the first target at 5 dB SNR, then others randomly in a similar way. So cases 1,2 and 3,4 are designed to see if random training or fixed SNR training is more effective. Case 5 trains and tests all targets with random SNRs from 0 to 10 dB. Case 6 trains all targets at 10 dB SNR and tests with one target at 5 dB SNR, and two or three targets at $10, 11, \cdots 20$ dB SNR. Finally test case 7 trains all targets at 5 dB SNR, and tests all targets with randomly selected SNRs from -10 to 10 dB.

The SNR in dB is calculated as $10log_{10}$ of the ratio of signal power to noise power. The noise is independent and identically distributed white Gaussian thermal noise.

Table 4.3: Experimental cases.

Case	**Training**	**Testing**
1	0: 20,000 1: 20,000 @ 10dB 2: 20,000 @ 10dB 3: 20,000 @ 10dB Total: 80,000	0: 20,000 1: 20,000 @ 10dB 2: 20,000 @ 10dB 3: 20,000 @ 10dB Total: 80,000

Table 4.3: (continued)

Case	Training	Testing
2	0: 20,000 1: 20,000 @ 10dB 2: 20,000 @ Rand[0,20] 3: 20,000 @ Rand[0,20] Total: 80,000	0: 20,000 1: 20,000 @ 10 dB 2: 20,000 @ Rand[0,20] 3: 20,000 @ Rand[0,20] Total: 80,000
3	0: 20,000 1: 20,000 @ 5 dB 2: 20,000 @ 5 dB 3: 20,000 @ 5 dB Total: 80,000	0: 20,000 1: 20,000 @ 5 dB 2: 20,000 @ Rand[0,20] dB 3: 20,000 @ Rand[0,20] dB Total: 80,000
4	0: 20,000 1: 20,000 @ 5 dB 2: 20,000 @ Rand[0,20] dB 3: 20,000 @ Rand[0,20] dB Total: 80,000	0: 20,000 1: 20,000 @ 5 dB 2: 20,000 @ Rand[0,20] dB 3: 20,000 @ Rand[0,20] dB Total: 80,000

Table 4.3: (continued)

Case	Training	Testing
5	0: 20,000 1: 20,000 @ Rand[0,10] dB 2: 20,000 @ Rand[0,10] dB 3: 20,000 @ Rand[0,10] dB Total: 80,000	0: 20,000 1: 20,000 @ Rand[0,10] dB 2: 20,000 @ Rand[0,10] dB 3: 20,000 @ Rand[0,10] dB Total: 80,000
6	0: 22,000 1: 22,000 @ 10 dB 2: 22,000 @ 10 dB 3: 22,000 @ 10 dB Total: 88,000	0: 22,000 1: 22,000 @ 5 dB 2: 22,000 @ 10:20 dB 3: 22,000 @ 10:20 dB Total: 88,000
7	0: 20,000 1: 20,000 @ 5 dB 2: 20,000 @ 5 dB 3: 20,000 @ 5 dB Total: 80,000	0: 20,000 1: 20,000 @ Rand[-10,10] dB 2: 20,000 @ Rand[-10,10] dB 3: 20,000 @ Rand[-10,10] dB Total: 80,000

4.6 Results and Discussion

Herein, as discussed above, synthesized radar returns from the same range bin are utilized in this study. Returns from different range bins can be processed separately (and similarly for range/Doppler processing). Thus restricting the returns to lie in the same range bin (but different azimuths) is a hard and challenging problem. Moreover, all the eigenvalue-based methods, such as AIC, MDL, Radoi's, etc. will fail here, since all of the target returns look exactly the same, except for their return amplitudes and the phase ramp across the array due to their azimuth location. So all of these methods are unsuitable for this application. To compare results, the proposed method is compared to MVDR. MVDR can analyze radar returns using a parameter sweep. The results are shown as confusion matrices, and also summarized in terms of the overall accuracy, the percentage of correct entries, underestimates and overestimates.

4.6.1 Training Parameters

Table 4.4 shows the training parameters used for the networks. Cases 5, 6 and 7 are more difficult so they utilized a larger learning rate and more epochs. A larger batch size was also utilized for better mini-batch variance estimates in these cases. In all cases, stochastic gradient descent with momentum [9] and a small L_2 regularization of 0.0001 was used for backpropagation. Some of the tests cases are easier (e.g. the network converges more quickly) than others, so the number of training times and epochs were empirically adjusted. The hardest cases (5–7) also utilized larger mini-batch sizes.

Table 4.4: Training parameters.

Case	Learning Rate	Momentum	Max. Epochs	Mini-batch Size
1	0.02	0.92	2	500
2	0.01	0.92	2	500
3	0.01	0.92	2	500
4	0.01	0.92	4	500
5	0.10	0.92	20	2,000
6	0.10	0.92	20	2,000
7	0.15	0.92	70	2,000

4.6.2 Test Case Analysis

Table 4.6 shows the confusion matrix and table 4.7 shows the overall results for case 1, respectively. From these tables, the network makes no mistakes with no targets or one target, and has a slight tendency to overestimate the targets. Table 4.6 can be interpreted as follows: The correct entries are across the diagonals, and the true number of targets are listed across the first row. When there are two targets, 19,816 were correctly identified as two targets, and 184 were mistaken for three targets. These mistakes can happen due to noise and overlapping distributions of the covariance matrix, and due to the interactions caused by target amplitude and location variations.

The results for the MVDR were not even comparable. Table 4.5 shows the confusion matrix for MVDR for case 1. The reason these results are poor are that the MVDR is really not able to discern multiple targets due to the small number of receivers, which has a very large Rayleigh resolution [56]. The results would improve and the MVDR would be able to resolve better with a larger number of receiver elements. Figure 4.4 shows two cases

of the MVDR response (normalized and plotted in dB), for two 10 dB targets located at azimuths $\phi_1 = 25^\circ$ and $\phi_2 = 28^\circ$. The noise level is 0 dB. In figure 4.4a, the MVDR estimate (plotted in dB) is shown for a 10-element receiver, and the response is plotted in figure 4.4b for a 41-element receiver. It is clear that MVDR is unable to discern the two targets clearly in the 10-element receiver case. Hereafter, cases present considerably harder results, and the MVDR results do not improve, so only the proposed method will be evaluated.

Table 4.5: MVDR Case 1 test confusion matrix.

	0	1	2	3
0	20,000	2,052	16,758	18,246
1	0	17,942	3,237	1,753
2	0	5	5	1
3	0	0	0	0

Table 4.6: Proposed Method Case 1 test confusion matrix.

	0	1	2	3
0	20,000	0	0	0
1	0	20,000	0	0
2	0	0	19,816	4
3	0	0	184	19,916

The results for test case 2 are shown in Tables 4.8 and 4.9. Case 2 shows that there were many errors between the two and three target cases, and that the testing data overall accuracies were much lower than those of the training data, indicating that the network was

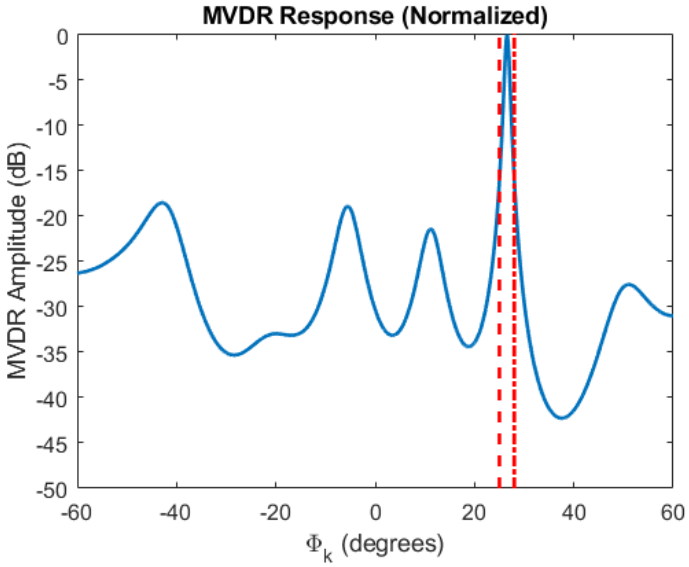

(a) MVDR response with 10 receiver elements.

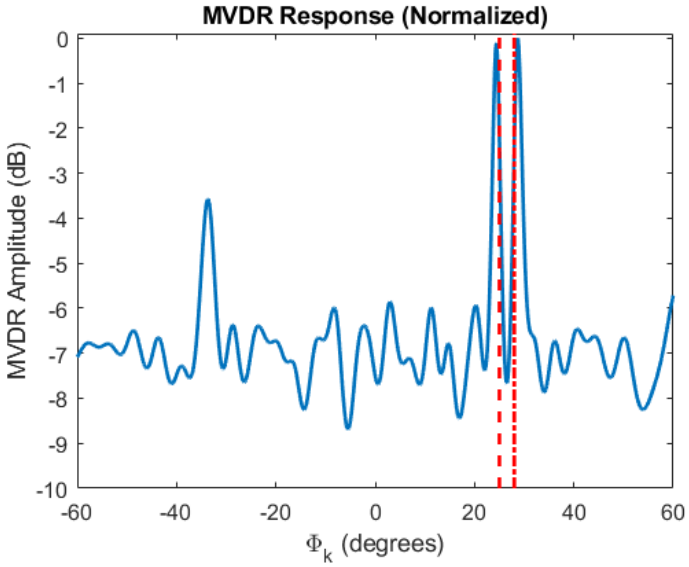

(b) MVDR response with 41 receiver elements.

Figure 4.4: MVDR plots (dB, normalized).

Note: Targets are 10 dB located at 25 and 28 degrees azimuth. The red lines indicate the true target locations. (a) 10-channel receiver. (b) 41-channel receiver.

Table 4.7: Proposed Method Case 1 overall results.

Case 1	Train	Test
Overall Accuracy (%)	99.769	99.765
Underestimated (%)	0.001	0.005
Overestimated(%)	0.230	0.230

over-trained. The results from test case 3 are listed in Tables 4.10 and 4.11. These results show that the network performed better when trained with a lower SNR target 1 (in case 3, this was 5 dB; in case 2, 10 dB).

Test case 4 was designed to see if using random SNR levels for the second and third targets versus constant levels would improve the results from case 3. This is clearly the case, as shown in Tables 4.12 and 4.13.

Test case 5, whose performance is summarized in 4.14 and 4.15 restricts the targets to 10 dB, and shows excellent results. Figure 4.5 shows a 2D histogram of the errors in test case 5, where the two dimensions are the second and third target SNR, respectively. The errors in this case are concentrated mostly at the lowest SNR values, as would be expected.

Test case 6 examines results by training all targets at 10 dB SNR, and varying the test case with a 5 dB SNR first target, and second and thirds targets varying from 10 to 20 dB SNR. The results are excellent, as shown in Tables 4.16 and 4.17.

Finally, in test case 7, the test scenario varies all three test targets randomly from -10 to 10 dB SNR, while the training is the same as test case 3, with all 5 dB SNR targets. The algorithm still performs very well, even with the low SNR values, as shown in Tables 4.18 and 4.19. Figure 4.6 shows a 2D histogram of the errors in test case 7, where the two dimensions are the second and third target SNR, respectively. As expected, the errors are

much lower towards the upper right of the figure, where the second and third target SNRs are higher, and increases in the bottom left, where the SNRs are both at their lowest values.

Table 4.8: Proposed Method Case 2 test confusion matrix.

	0	1	2	3
0	20,000	0	0	0
1	0	20,000	5,401	937
2	0	0	6,585	4,321
3	0	0	8,014	14,742

Table 4.9: Proposed Method Case 2 overall results.

Case 2	Train	Test
Overall Accuracy (%)	99.981	76.659
Underestimated (%)	0.000	13.324
Overestimated(%)	0.019	10.018

Table 4.10: Proposed Method Case 3 test confusion matrix.

	0	1	2	3
0	20,000	0	0	0
1	0	19,999	1,118	7
2	0	1	5,851	913
3	0	0	13,031	19,080

Table 4.11: Proposed Method Case 3 overall results.

Case 3	Train	Test
Overall Accuracy (%)	99.954	81.163
Underestimated (%)	0.019	2.548
Overestimated(%)	0.028	16.290

Table 4.12: Proposed Method Case 4 test confusion matrix.

	0	1	2	3
0	20,000	0	0	0
1	0	19,994	555	2
2	0	6	17,400	4,913
3	0	0	2,045	15,084

Table 4.13: Proposed Method Case 4 overall results.

Case 4	Train	Test
Overall Accuracy (%)	91.203	90.597
Underestimated (%)	6.545	6.839
Overestimated(%)	2.252	2.564

Table 4.14: Proposed Method Case 5 test confusion matrix.

	0	1	2	3
0	20,000	0	0	0
1	0	19,865	422	4
2	0	135	18,352	2,414
3	0	0	1,226	17,582

Table 4.15: Proposed Method Case 5 overall results.

Case 5	Train	Test
Overall Accuracy (%)	95.539	94.749
Underestimated (%)	3.076	3.550
Overestimated(%)	1.385	1.701

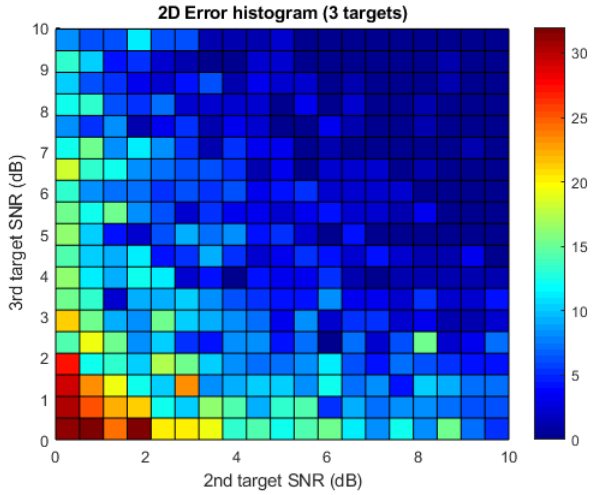

Figure 4.5: 2D histogram of errors in case 5. Best viewed in color.

Table 4.16: Proposed Method Case 6 test confusion matrix.

	0	1	2	3
0	20,000	0	0	0
1	0	21,999	300	2
2	0	1	21,684	411
3	0	0	16	21,587

Table 4.17: Proposed Method Case 6 overall results.

Case 6	Train	Test
Overall Accuracy (%)	99.294	99.170
Underestimated (%)	0.699	0.810
Overestimated(%)	0.007	0.019

Table 4.18: Proposed Method Case 7 test confusion matrix.

	0	1	2	3
0	20,000	0	0	0
1	0	19,557	1,306	38
2	0	443	14,710	5,126
3	0	0	3,984	14,836

Table 4.19: Proposed Method Case 7 overall results.

Case 1	Train	Test
Overall Accuracy (%)	89.230	86.379
Underestimated (%)	6.689	8.088
Overestimated(%)	4.081	5.534

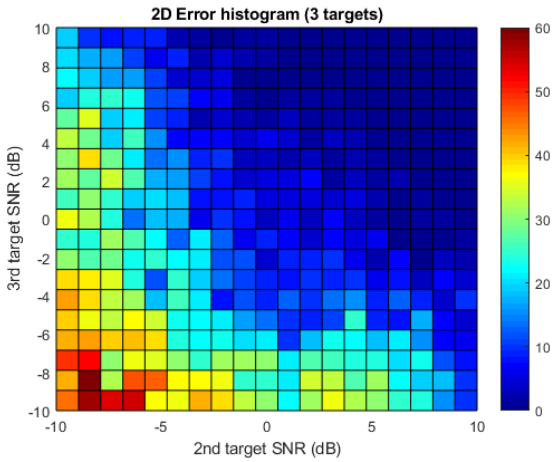

Figure 4.6: 2D histogram of errors in case 7. Best viewed in color.

4.6.3 Architectural Trade–offs

One question to be answered is "how deep of a network is required?" To assess this, the number of network layers was varied. Table 4.20 show the different configurations. Table 4.21 shows the training and testing results for data case 6 for the four networks shown in table 4.20. From Table 4.21, the proposed network provided the best results. As the number of layers was reduced, so was the performance of the network. Comparing network 1 (the proposed network) to network 4 (which has no dropout), the results were significantly lower for network 4. This indicates that the dropout forced network 1 to train more robustly [53].

Table 4.20: Deep network architectures. NW 1 is the proposed network.

	NW 1	**NW 2**	**NW 3**	**NW 4**
Num Layers	15	12	9	14
1	FC	FC	FC	FC
2	PReLU	PReLU	PReLU	PReLU
3	BN	BN	BN	BN
4	FC	FC	DR	FC
5	PReLU	PReLU	FC	PReLU
6	BN	BN	PReLU	BN
7	FC	DR	BN	FC
8	PReLU	FC	SM	PReLU
9	BN	PReLU	CL	BN
10	DR	BN	-	FC
11	FC	SM	-	PReLU
12	PReLU	CL	-	BN
13	BN	-	-	SM
14	SM	-	-	CL
15	CL	-	-	-

Table 4.20: (continued)

Note: FC = Fully Connected, PReLU = Parametric ReLU, BN = Batch Normalization, DR = Dropout, SM = Softmax, CL = Classifier, NW = Network.

Table 4.21: Architectural results on data for Case 6.

	NW 1	NW 2	NW 3	NW 4
Train Acc (%)	**99.294**	97.758	84.409	96.988
Test Acc (%)	**99.170**	97.715	84.165	96.697

Note: NW = Network. The networks are defined in Table 4.20.
The best results are in **bold**.

Another question to be answered is "how will the network perform with only the covariance matrix or eigenvalues as inputs?" In order to address this question, the network was modified for (1) the covariance matrix only (input vector size of 100), and (2) eigenvalues only (input vector size of 10). The results are shown in Table 4.22. From this table, it is clear that the eigenvalues are basically useful for separating the cases of noise only from the case of one or more targets. Moreover, the best results occur when the covariance matrix plus the eigenvalues are used. This justifies using both of these inputs.

4.7 Conclusion

Standard solutions for estimating the number of sources, such as MVDR, MUSIC, AIC and MDL all fail in cases where the signals present do not spread into multiple eigenvalues of the data covariance matrix. However, the eigenvalues do contain information that can be

Table 4.22: Comparison of results for case 6 with different input combinations.

Inputs (dim)	EIG (10)		COV (200)		COV+EIG (210)	
	Train	Test	Train	Test	Train	Test
OA (%)	60.649	60.555	99.157	98.982	**99.294**	**99.170**
UE (%)	18.608	18.684	0.787	0.936	**0.699**	**0.810**
OE (%)	20.743	20.761	0.056	0.082	**0.007**	**0.019**

Note: COV = Covariance matrix only (split into real and imaginary), EIG = eigenvalues only, COV + EIG = Covariance matrix plus eigenvalues. OA = Overall Accuracy, UE = Underestimated, OE = Overestimated. Best results in **bold**.

used to estimate the number of sources. Moreover, combining eigenvalues and covariance matrix data and utilizing a deep network allows very robust estimation of the number of sources, even when all of the sources are at the same range bin. The proposed deep learning system which fuses the covariance matrix and eigenvalues was found to accurately estimate the number of sources, even when the number of receiver channels is small and the number of pulses is also modest. The optimal network depth was found to be 15 layers, and the system could estimate very closely–spaced (in azimuth) and very small (in terms of SNR) targets (down to -10 dB). This is an important contribution, because signal-subspace methods such as MUSIC and MLE require $apriori$ estimates of the number of sources. Also, the proposed method does not require matrix inversion (or adding diagonal loading to make the covariance matrix better conditioned, and thus artificially inflating the noise floor).

The proposed method worked well, even at low SNR values. There could be potential electronic countermeasure (ECM) applications, such as detecting how many low power radars are operating in an area. There is also potential for non–radar applications, such as

modifying the method to not only estimate the number of sources, but also to estimate the relative SNRs of the different sources. This would require adding additional NN regression modules. This approach could have many applications in wireless communications,such as estimating the number of radios talking simultaneously on a channel.

Future work includes (1) analyzing the network in the presence of receiver alignment errors, phase and amplitude mismatches, (2) extending the results to wide-bandwidth signals, and (3) investigating denoising techniques (denoise the inputs before using the network), (4) extending the work to also estimate the AOA of the sources, (5) extending the solution from a uniform linear array to a 2D array, and (6) utilizing a complex–valued NN to process the data.

CHAPTER V

CONCLUSIONS

5.1 Conclusions

Array signal processing techniques which are prominent in the literature hold a strong bias towards uniform array geometries and narrowband signals. Though current research is being done to expand DOA processing techniques for arbitrary arrays and wideband signals, there still exist areas lacking complete and robust solutions for DOA estimation.

Chapter III highlighted some of the pitfalls with existing techniques for DOA estimation on conformal arrays for wideband acoustic signals, which included lack of methods designed for such an application. It was further explored if sub array geometries could be utilized to expand the algorithms available, though this study was inconclusive.

Chapter IV exposed a problematic area for number of source estimations in a radar application where all targets exist in the same range bin. To the best of my knowledge, there have been no solutions developed to account for this situation. Thus, a deep NN approach was developed to handle this particular case and has shown promising results for future usage.

This thesis exposes lacking areas in the field of direction of arrival estimation as well as provides building blocks to begin filling those gaps. While a novel DOA estimation technique was not developed, a method to estimate the number of sources was. This ap-

proach shows promising results which will enable algorithms that need this estimate to have improved accuracies.

5.2 For Further Research

Because of the additional complexities that wideband acoustic signals introduce over narrowband radar signals, clearly the next step is extending the deep learning approach for number of source detections into the acoustic realm. On the same note, because estimating the number of sources is a precursor to estimating an angle or direction of arrival, extending the number of source estimation technique to DOA methods which are based on this a priori knowledge will yield a significant contribution to the field.

REFERENCES

[1] "Sound," *Funk Wagnalls New World Encyclopedia*, 2017, p. 1.

[2] D. Aalfs, *Adaptive Array Radar Processing (Professional Education)*, Georgia Tech Research Institute, 2011.

[3] M. Agatonovic, Z. Stankovic, I. Milovanovic, N. Doncov, L. Sit, T. Zwick, and B. Milovanovic, "Efficient neural network approach for 2D DOA estimation based on antenna array measurements," *Progress In Electromagnetics Research*, vol. 137, 2013, pp. 741–758.

[4] H. Akaike, "A new look at the statistical model identification," *IEEE transactions on automatic control*, vol. 19, no. 6, 1974, pp. 716–723.

[5] S.-i. Amari and A. Cichocki, "Adaptive blind signal processing-neural network approaches," *Proceedings of the IEEE*, vol. 86, no. 10, 1998, pp. 2026–2048.

[6] P. Annibale and R. Rabenstein, "Closed-form estimation of the speed of propagating waves from time measurements," *Multidimensional Systems and Signal Processing*, vol. 25, no. 2, Apr 2014, pp. 361–378.

[7] S. J. Axler, *Linear algebra done right*, vol. 2, Springer, 1997.

[8] L. Badidi and L. Radouane, "A Neural Network Approach for DOA Estimation and Tracking," *Proceedings of the Tenth IEEE Workshop on Statistical Signal and Array Processing, 2000*, 2000, pp. 434–438.

[9] C. M. Bishop, *Pattern recognition and machine learning (information science and statistics)*, Springer–Verlag, 2006.

[10] S. Çaylar, K. Leblebicioğlu, and G. Dural, "A new neural network approach to the target tracking problem with smart structure," *Radio science*, vol. 41, no. 5, 2006.

[11] P.-R. Chang, W.-H. Yang, and K.-K. Chan, "A Neural Network Approach to MVDR Beamforming Problem," *IEEE Transactions on Antennas and Propagation*, vol. 34, no. 11, 1986, pp. 8190–8192.

[12] C. E. Chen, F. Lorenzelli, R. E. Hudson, and K. Yao, "Maximum Likelihood DOA Estimation of Multiple Wideband Sources in the Presence of Nonuniform Sensor Noise," *EURASIP Journal on Advances in Signal Processing*, vol. 2008, no. 1, Nov 2007, p. 835079.

[13] G. Cybenko, "Approximation by superpositions of a sigmoidal function," *Mathematics of Control, Signals, and Systems (MCSS)*, vol. 2, no. 4, 1989, pp. 303–314.

[14] K.-L. Du, A. Lai, K. Cheng, and M. Swamy, "Neural methods for antenna array signal processing: a review," *Signal Processing*, vol. 82, no. 4, 2002, pp. 547–561.

[15] A. EL Zooghby, H. Southall, and C. Christodoulou, "Experimental validation of a neural network direction finder," *Antennas and Propagation Society International Symposium, 1999. IEEE*. IEEE, 1999, vol. 3, pp. 1592–1595.

[16] A. H. El Zooghby, "Performance of radial-basis function networks for direction of arrival estimation with antenna arrays," *IEEE Transactions on Antennas and Propagation*, vol. 45, no. 11, 1997, pp. 1611–1617.

[17] A. H. El Zooghby, C. G. Christodoulou, and M. Georgiopoulos, "A neural network-based smart antenna for multiple source tracking," *IEEE Transactions on Antennas and Propagation*, vol. 48, no. 5, 2000, pp. 768–776.

[18] A. H. El Zooghby, C. G. Christodoulou, and M. Gerogiopoulos, "Neural Network-based Adaptive Beamforming For One- And Two-dimensional Antenna Arrays," *IEEE Transactions on Antennas and Propagation*, vol. 46, no. 12, 1999, pp. 1997–1999.

[19] N. J. G. Fonseca, M. Coudyser, J.-J. Laurin, and J.-J. Brault, "On the Design of a Compact Neural Network-Based DOA Estimation System," *IEEE Transactions on Antennas and Propagation*, vol. 58, no. 2, 2010, pp. 357–366.

[20] E. Gorman, S. Bunkley, J. E. Ball, and A. Netchaev, "Direction of arrival estimation for conformal arrays on real-world impulsive acoustic signals," *Proceedings of Meetings on Acoustics*, vol. 31, no. 1, 2017, p. 055003.

[21] E. Gorman, J. Rogers, J. E. Ball, and N. Egger, "Robust estimation of the number of radar signal sources using deep learning," 2018.

[22] E. M. Grais, M. U. Sen, and H. Erdogan, "Deep neural networks for single channel source separation," *Acoustics, Speech and Signal Processing (ICASSP), 2014 IEEE International Conference on*. IEEE, 2014, pp. 3734–3738.

[23] H. He, T. Li, T. Yang, and L. He, "Direction of arrival (DOA) estimation algorithm based on the radial basis function neural networks," *Advances in Multimedia, Software Engineering and Computing Vol. 1*, Springer, 2011, pp. 389–394.

[24] K. He, X. Zhang, S. Ren, and J. Sun, "Delving deep into rectifiers: Surpassing human-level performance on imagenet classification," *Proceedings of the IEEE International Conference on Computer Vision*, 2015, pp. 1026–1034.

[25] A. Hirose, *Complex-valued neural networks: theories and applications*, vol. 5, World Scientific, 2003.

[26] A. Hirose, *Complex-valued neural networks: Advances and applications*, vol. 18, John Wiley & Sons, 2013.

[27] Y. Huang, J. Benesty, G. W. Elko, and R. M. Mersereati, "Real-time passive source localization: a practical linear-correction least-squares approach," *IEEE Transactions on Speech and Audio Processing*, vol. 9, no. 8, Nov 2001, pp. 943–956.

[28] S. Ioffe and C. Szegedy, "Batch normalization: Accelerating deep network training by reducing internal covariate shift," *arXiv preprint arXiv:1502.03167*, 2015.

[29] P. Jarske, T. Saramaki, S. K. Mitra, and Y. Neuvo, "On properties and design of nonuniformly spaced linear arrays [antennas]," *IEEE Transactions on Acoustics, Speech, and Signal Processing*, vol. 36, no. 3, Mar 1988, pp. 372–380.

[30] S. Jha and T. Durrani, "Direction of arrival estimation using artificial neural networks," *IEEE Transactions on Systems, Man and Cybernetics*, vol. 21, no. 5, 1991, pp. 1192–1201.

[31] O. d. A. D. Júnior, A. D. D. Neto, and W. da Mata, "Determination of multiple direction of arrival in antennas arrays with radial basis functions," *Neurocomputing*, vol. 70, no. 1, 2006, pp. 55–61.

[32] S. Kiani and A. M. Pezeshk, "A Comparative Study of Several Array Geometries for 2D DOA Estimation," *Procedia Computer Science*, vol. 58, no. Supplement C, 2015, pp. 18 – 25, Second International Symposium on Computer Vision and the Internet (VisionNet15).

[33] Y. Kim and H. Ling, "Direction of arrival estimation of humans with a small sensor array using an artificial neural network," *Progress In Electromagnetics Research B*, vol. 27, 2011, pp. 127–149.

[34] L. E. Kinsler, *Fundamentals of acoustics*, John Wiley Sons, 2000.

[35] C. Knapp and G. Carter, "The generalized correlation method for estimation of time delay," *IEEE Transactions on Acoustics, Speech, and Signal Processing*, vol. 24, no. 4, Aug 1976, pp. 320–327.

[36] H. Krim and M. Viberg, "Two decades of array signal processing research: the parametric approach," *IEEE signal processing magazine*, vol. 13, no. 4, 1996, pp. 67–94.

[37] Z. Le, *Research on direction of arrival estimation algorithm in smart antenna*, doctoral dissertation, South China University of Technology, Guangzhou China, 2010.

[38] T. Lo, H. Leung, and J. Litva, "Radial Basis Function Neural Network for Direction-of-Arrivals Estimation," *IEEE Signal Processing Letters*, vol. 1, no. 2, 1994, pp. 45–47.

[39] K. Matsuoka, M. Ohoya, and M. Kawamoto, "A neural net for blind separation of nonstationary signals," *Neural networks*, vol. 8, no. 3, 1995, pp. 411–419.

[40] S. Mohan, M. E. Lockwood, M. L. Kramer, and D. L. Jones, "Localization of multiple acoustic sources with small arrays using a coherence test," *The Journal of the Acoustical Society of America*, vol. 123, no. 4, 2008, p. 21362147.

[41] G. Ofek, J. Tabrikian, and M. Aladjem, "A modular neural network for direction-of-arrival estimation of two sources," *Neurocomputing*, vol. 74, no. 17, 2011, pp. 3092–3102.

[42] T. Pham and B. M. Sadler, "Aeroacoustic wideband array processing for detection and tracking of ground vehicles," *The Journal of the Acoustical Society of America*, vol. 98, no. 5, 1995, pp. 2969–2969.

[43] E. Radoi and A. Quinquis, "A new method for estimating the number of harmonic components in noise with application in high resolution radar," *EURASIP Journal on Advances in Signal Processing*, vol. 2004, no. 8, 2004, p. 615890.

[44] J. Rissanen, "Modeling by shortest data description," *Automatica*, vol. 14, no. 5, 1978, pp. 465–471.

[45] R. Roy and T. Kailath, "ESPRIT-estimation of signal parameters via rotational invariance techniques," *IEEE Transactions on acoustics, speech, and signal processing*, vol. 37, no. 7, 1989, pp. 984–995.

[46] S. Santosh, O. P. Sahu, and M. Aggarwal, "Different Wideband Direction of Arrival(DOA) Estimation methods: An Overview," *Proceedings of the 8th WSEAS Int. Conf. on ELECTRONICS, HARDWARE, WIRELESS and OPTICAL COMMUNICATIONS*, p. 1725.

[47] M. Sarevska, B. Milovanovic, and Z. Stankovic, "Alternative signal detection for neural network-based smart antenna," *Neural Network Applications in Electrical Engineering, 2004. NEUREL 2004. 2004 7th Seminar on*. IEEE, 2004, pp. 85–89.

[48] M. Sarevska, B. Milovanovic, and Z. Stankovic, "Reliability of the hidden layer in neural network smart antenna.," *WSEAS Transactions on Circuits and Systems*, vol. 4, no. 8, 2005, pp. 556–563.

[49] R. Schmidt, "Multiple emitter location and signal parameter estimation," *IEEE transactions on antennas and propagation*, vol. 34, no. 3, 1986, pp. 276–280.

[50] C.-s. Shieh and C.-t. Lin, "Direction of Arrival Estimation Based on Phase Differences Using Neural Fuzzy Network," *IEEE Transactions on Antennas and Propagation*, vol. 48, no. 7, 2000, pp. 1115–1124.

[51] M. Solazzi, F. Piazza, and A. Uncini, "Nonlinear blind source separation by spline neural networks," *Acoustics, Speech, and Signal Processing, 2001. Proceedings.(ICASSP'01). 2001 IEEE International Conference on*. IEEE, 2001, vol. 5, pp. 2781–2784.

[52] H. Southall, J. A. Simmers, and T. H. O'Donnell, "Direction Finding in Phased Arrays with a Neural Network Beamformer," *IEEE Transactions on Antennas and Propagation*, vol. 43, no. 12, 1995, pp. 1369–1374.

[53] N. Srivastava, G. E. Hinton, A. Krizhevsky, I. Sutskever, and R. Salakhutdinov, "Dropout : A Simple Way to Prevent Neural Networks from Overfitting," *Journal of Machine Learning Research (JMLR)*, vol. 15, no. 1, 2014, pp. 1929–1958.

[54] Y. Tan, J. Wang, and J. M. Zurada, "Nonlinear blind source separation using a radial basis function network," *IEEE transactions on neural networks*, vol. 12, no. 1, 2001, pp. 124–134.

[55] T. E. Tuncer and B. Friedlander, *Classical and modern direction-of-arrival estimation*, Acad Pr., 2009.

[56] H. L. Van Trees, *Optimum array processing: Part IV of detection, estimation and modulation theory*, vol. 1, Wiley Online Library, 2002.

[57] F. Vesperini, P. Vecchiotti, E. Principi, S. Squartini, and F. Piazza, "Localizing Speakers in Multiple Rooms by Using Deep Neural Networks," *Computer Speech & Language*, 2017.

[58] M. Wang, S. Yang, S. Wu, and F. Luo, "A RBFNN approach for DoA estimation of ultra wideband antenna array," *Neurocomputing*, vol. 71, no. 4, 2008, pp. 631–640.

[59] M. Wax and T. Kailath, "Detection of signals by information theoretic criteria," *IEEE Transactions on Acoustics, Speech, and Signal Processing*, vol. 33, no. 2, 1985, pp. 387–392.

[60] W. H. Yang, K. K. Chan, and P. R. Chang, "Complex-valued neural network for direction of arrival estimation," *Electronics Letters*, vol. 30, no. 7, 1994, pp. 2–3.

[61] Y.-S. Yoon, L. Kaplan, and J. McClellan, "Direction-of-arrival estimation of wideband sources using arbitrary shaped multidimensional arrays," vol. 2, 06 2004, pp. ii – 221.

[62] P. Yu and L. Wang, "Wideband DOA estimation by using off-grid technique for a cylindrical conformal array," *2016 CIE International Conference on Radar (RADAR)*, Oct 2016, p. 14.

[63] X. Zhang, R. Cao, and J. G. Webster, *Direction of Arrival Estimation: Introduction*, John Wiley Sons, Inc., 1999.

[64] Y. Zhang, Z. Gong, and Y. Sun, "DOA estimation in smart antenna based on general regression neural network," *Journal of Military Communications Technology*, vol. 28, no. 1, 2007, pp. 23–25.

[65] I. Ziskind and M. Wax, "Maximum likelihood estimation via the alternating projection maximization algorithm," *Acoustics, Speech, and Signal Processing, IEEE International Conference on ICASSP'87.* IEEE, 1987, vol. 12, pp. 2280–2283.

[66] lk Baysal and O. L. Moses, "Optimal Array Geometries for Wideband DOA Estimation,".